AN ABSTRACT OF THE THESIS OF

Yuhao Chang for the degree of Master of Science in Electrical and Computer Engineering presented on March 24, 2006.

Title: A Channelized Digital Receiver Design for UWB Systems in a Multipath Indoor Environment

Abstract approved:

Mario E. Magaña

This thesis presents a channelized digital receiver design for UWB sytems in a multipath indoor environment. The UWB technology has been used for commercial and military purposes due to a number of advantages such as low-power consumption, noise-like and carrier free. The energy of UWB signal is spread over a wide range from near d.c. to a few gigahertz. For this reason, the analog to digital converter (ADC) in the receiver must support an extremely high sampling frequency (at least Nyquist rate) and high resolution. By using a channelized digital receiver, the speed of ADC can be considerably relaxed. The received signal is split into several subbands and sampled at a fraction rate of sampling frequency.

In multipath environments, we propose a receiver architecture which provides a robust immunity to multipath interference. The proposed receiver consists a collection of receivers. If the multipath signal energy increases, the decision can be made more accurate.

A Channelized Digital Receiver Design for UWB Systems in a Multipath Indoor Environment

by
Yuhao Chang

A THESIS

submitted to

Oregon State University

in partial fulfillment of
the requirements for the
degree of

Master of Science

Presented March 24, 2006
Commencement June 2006

Master of Science thesis of Yuhao Chang
presented on March 24, 2006.

APPROVED:

_____

Major Professor, Electrical and Computer Engineering

_____

Associate Director of the School of Electrical Engineering and Computer Science

_____

Dean of the Graduate School

I understand that my thesis will become part of the permanent collection of Oregon State University libraries. My signature below authorizes release of my thesis to any reader upon request.

_____

Yuhao Chang, Author

ACKNOWLEDGEMENTS

This thesis is for my parents. Without their support, I can't finish it. I hope that my dad could know that I am done with it. In addition, I would like to thank for my advisor, Dr. Mario E. Magaña who have always instructed me and gave me advice about not only my research but also matters handling for life. I do appreciate it

I would like to thank Panupat Poocharoen, Robert Istvan Bogya and Guy Barnes Jr. for their appropriate suggestions as well.

TABLE OF CONTENTS

TABLE OF CONTENTS (Continued)

LIST OF FIGURES

Figure Page

LIST OF FIGURES (Continued)

Figure Page

LIST OF FIGURES (Continued)

Figure Page

LIST OF FIGURES (Continued)

Figure Page

A Channelized Digital Receiver Design for UWB Systems in A Multi-path Indoor Environment

1. Introduction

Ultra wideband (UWB) communication technology has been used for both military and commercial purposes. UWB systems transmit information data over a wide frequency spectrum with low power consumption and high speed for local area wireless network applications. Unlike the traditional digital communication method based on a carrier wave, UWB may be pulse based.

Since an UWB signal has a "low probability of detection" it has been often used in military applications. In addition, if non-related parties try to listen in, they will only hear what amounts to background noise. Recently, there have been some UWB applications such as Ground Penetrate Radar (GPR) applications, which are being used for precise measurement of distance and wireless communications.

In its application, UWB usually coexists with other narrow band radio systems. These narrow band signals often interfere with one and other, yet by employing spread-spectrum techniques. UWB is much less susceptible to interference. Both direct-sequence spread-spectrum (DSSS) and time hopping spread-spectrum are popular and simple schemes considered for UWB systems. For this thesis, there is only one user in the UWB environment so we are not concerned about spread-spectrum techniques.

Because there exist limits caused by circuit nonidealities and circuit mismatches, it is helpful to digitize the received UWB signals to achieve high performance and avoid using as many analog elements in the UWB receiver. Most of the operations of the system could be performed digitally and efficiently by means of sampling the UWB signals using the Nyqusit rate. Due to the several gigahertz required sampling rate, we need to design very high-speed ADCs. Yet this is a very challenging task, even when we take into account the great advances in COMS technology so far. Currently, ADCs can have 8 bits resolution at 1.5 GSPS [1][20].

Nevertheless, we still need to take the prohibitive cost of implementation into consideration.

An alternative solution would be to use a channelized receiver [2][3][4][5]. By using a filter bank and multiplexers that split the full band into several subchannels, the sampling frequency can be reduced. Each of the subchannels is sampled at a fraction of the effective sampling frequency. The received UWB signal passes through a bank of analysis filters which is composed of sharp low pass filters and multiplexers. Although it can be implemented by bank of band pass filters, it is difficult to design sharp band pass filters with high center frequency.

In using a hybrid filter bank (HFB) [5][6][7][8], we employ continuous-time analog analysis filters and discrete-time synthesis filters. However, the transmitted signals are not reconstructed perfectly in the final synthesis. Instead, the information and data are collected from each branch of the system and then the optimal transmitted signals for data detection are estimated. The challenge in constructing an HFB is to design the analog and digital filters in the filter bank that provide an accurate reconstruction of transmitted signal. To minimize the effects of maulitpaths, narrowband interference, and distortions such as phase distortion, amplitude distortions, aliasing distortions introduced by HFB itself, we need to design filters with good characteristics. Nevertheless, the distortion caused by propagation channels and analysis filters can be dealt with by employing adaptive synthesis filters to recover the transmitted signals [2][3][4][5]. The synthesis filters here perform a combination of match filtering, channel estimation, aliasing cancellation, etc.. Unfortunately a drawback of most synthesis filters is their slow convergence. Since the convergence rate depends on the selected converge parameter and signal conditions. In the time-varying channel case, the convergence speed may not be fast enough. Since many papers have already been devoted to this problem we will not belabor this point further [18].

In a multipath propagation environment, the transmitted signals arrive at the receiver via multipaths at different propagation delays and different attenuations [19]. To suppress any interference, we design receivers corresponding to each path. If the multipath signal energy increases, the decision device can be more accurate in its

decision making. In our indoor environment, the signal fading coefficients are time-invariant over the symbol interval. Our focus is solely concerned with the reflection from the ground and walls. The Doppler spread is not considered because of slow mobility. A number of works that deal with UWB signals over multipath channel have been published [21]. It is known that the rake receiver technique is an effective solution for this scenario. This technique uses several correlators which process several multipath components individually. The outputs of the correlators are then combined according to some design criterion, in order to achieve better BER performance and reliability.

Specifically, this thesis focuses on a channelized UWB receiver design for an indoor environment. To better understand the approach herein presented, some basic theory of UWB and system model will be presented fist. The thesis is organized as follow:

In Chapter 2, the fundamental theory behind UWB is briefly presented, including the pulse shape and spectrum of UWB. Furthermore, the Federal Communications Commission (FCC) regulations concerning the spectrum and power level will also be discussed.

In Chapter 3, UWB signals are modulated for transmission. There are some popular modulation types which have been used widely for UWB system. Each of them will be summarized and their advantages/disadvantages discussed.

In Chapter 4, our proposed system model is presented. The transmitter, channel model and receiver are discussed. The block diagram of the whole system will be presented later in order to help us further understand the data processing in our system.

In Chapter 5, we provide the Matlab simulation results showing that bit error rate (BER) can be improved by means of applying a simple encoder to the proposed receiver. In addition, this system is analyzed in this chapter.

Finally, in Chapter 6, conclusions and open problems are presented.

2. UWB Communications

In this chapter, the fundamental theory for UWB communications will be briefly discussed. We will consider the mechanism used to generate the UWB pulse and take a look at its corresponding UWB spectrum. Additionally, FCC rules for indoor UWB devices are presented.

2.1 FCC Ruling

Currently, UWB technologies are being deployed in today's wireless world. Recognizing the potential advantage of UWB, the FCC set down regulations regarding UWB spectrum occupancy and power levels. They are described as follow [15]:

- The fractional bandwidth of UWB is greater than 25% or occupies 1.5GHz or more of spectrum. The fraction bandwidth is defined as $2(f_H-f_L)/(f_H+f_L)$, where f_H is the upper frequency of the -10 dB emission point and f_L is the lower frequency of the -10 dB emission point. The center frequency of the transmission was defined as the average of the upper and lower -10 dB points.

- UWB transmission can legally range from 3.1 GHz to 10.6 GHz.

- The power of an indoor UWB device must fit those limits:
  - -41.3dBm between 3.1-10.6 GHz and below 1 GHz
  - -51 dBm between 2-3.1 GHz and above 10.6 GHz
  - -75 dBm between 1-1.6 GHz

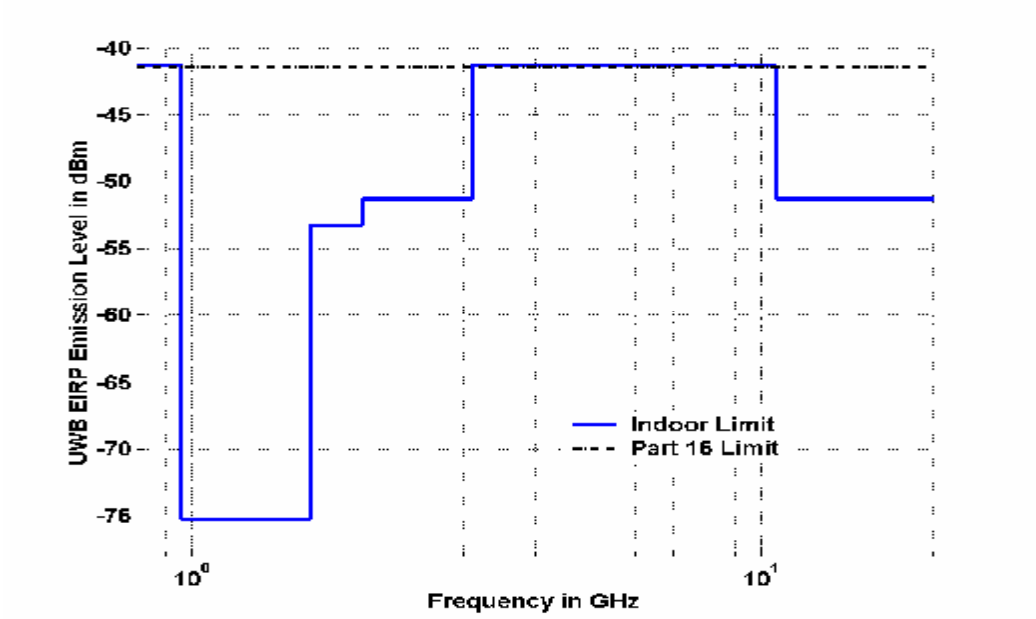

Figure2.1 UWB Spectrum Mask

2.2 UWB Pulse Generation Theory

Prior to constructing an ultra wide band pulse, we need to determine the desired pulse shape. The most popular pulse shape for UWB communication system is the Gaussian pulse. For transmission, we usually employ the Gaussian monocycle. It is the first derivative of a Gaussian pulse. In principle, a baseband UWB pulse is carrier free, the carrier frequency is employed in here to meet the FFC's spectrum mask. Combining the Guassion pulse with a sinusoidal carrier with 6.85 GHz carrier frequency, we can easily obtain an UWB pulse for transmission.

The Guassion pulse can be described by:

$$S_g(t) = e^{-2p(\frac{2t}{0.1T})^2} \qquad (2.1)$$

where, T = 6.25ns is cycle duration

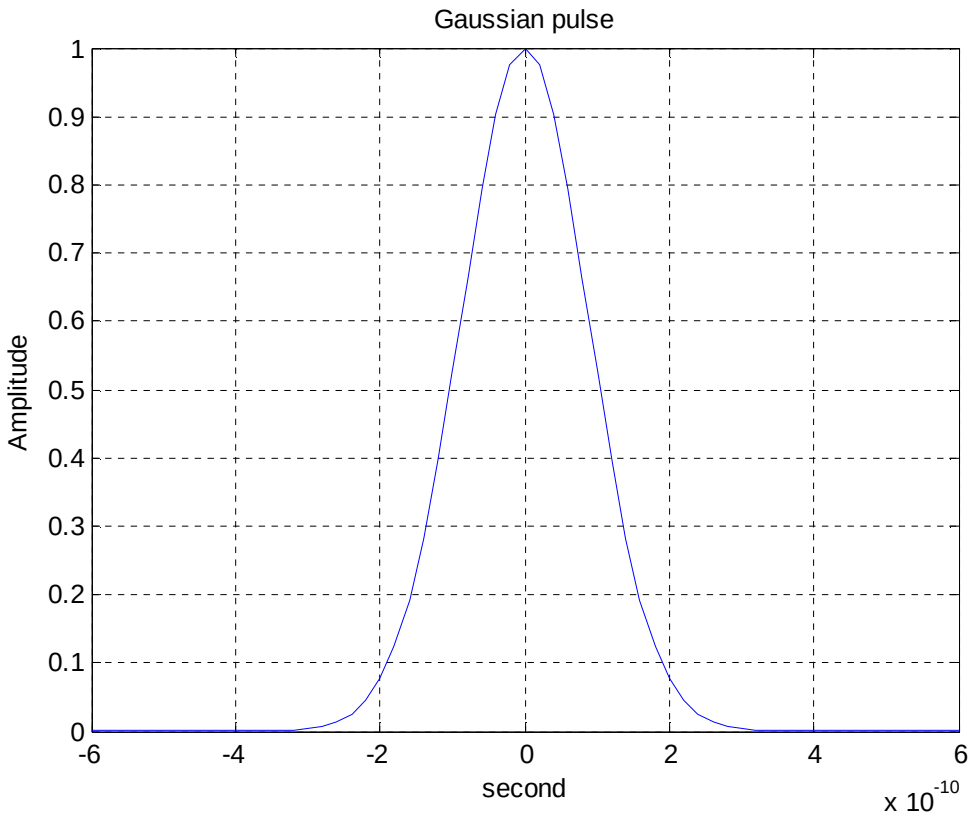

Figure 2.2.1 Gaussian pulse

The next step is to generate the transmitted UWB pulse. Equation (2.1) above is then multiplied by sinusoidal carrier to get a bandpass UWB pulse. It is described by:

$$S_{uwb}(t) = A * e^{-2p(\frac{2t}{0.1T})^2} * \sin(wt) \qquad (2.2)$$

Where, $\omega = 2\pi f$

f = 6.85 GHz (carrier frequency)

A = 0.0006 V (amplitude)

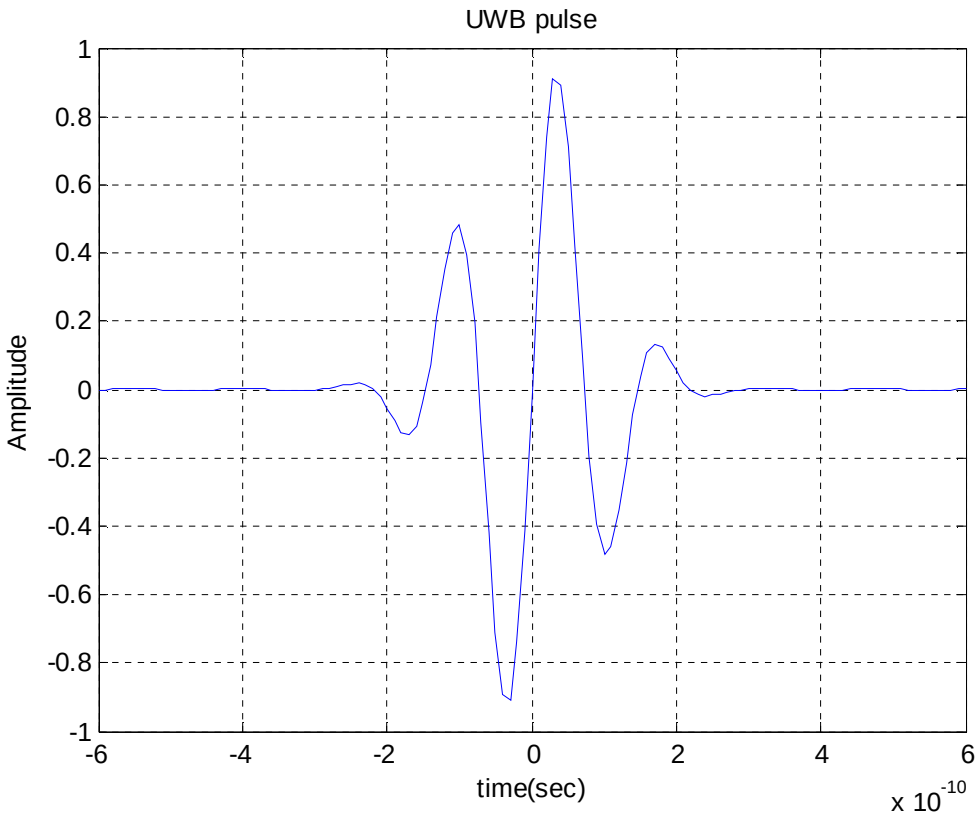

Figure 2.2.2 UWB pulse

By adjusting the value of A, the power spectral density of the UWB pulse stream can be made to meet the FCC regulations. As seen in figure 2.2.2, UWB signals have very short duration (< 1ns) but have a wide bandwidth over several gigahertz.

Generally, the first derivative of a Gaussian pulse, called a monocycle Gaussian pulse is used in UWB communication. It is illustrated in Figure 2.2.3. The mathematical representation of monocycle Gaussian pulse is given by [10]:

$$S_{monocycle} = C * t * e^{-2p(\frac{t}{t})^2} \qquad (2.2.3)$$

Where, C is an amplitude constant

t is a time delay constant associated with width of pulse.

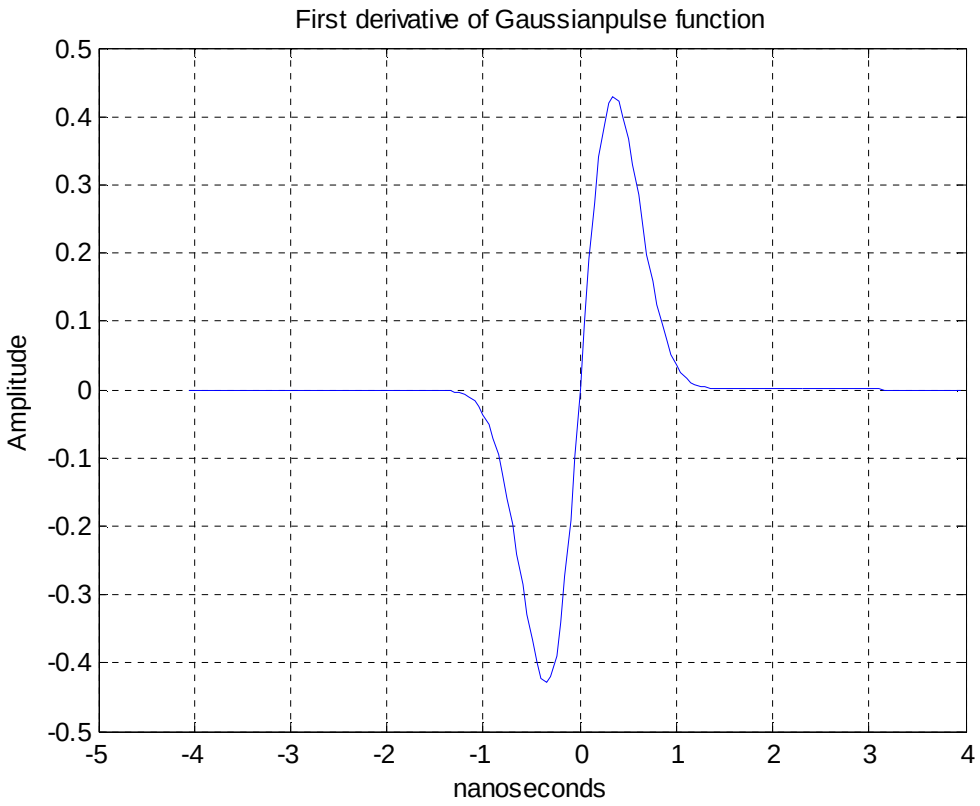

Figure 2.2.3 Gaussian Monocycle pulse

2.3 UWB Spectrum

There are some different limits between indoor and outdoor systems. A power spectral density mask can show those limits. For an indoor UWB application, the power spectral density is -41.3 dBm from 3.1 GHz to 10.6 GHz, -51 dBm from 2 GHz to 3.1 GHz, and -75 dBm from 1 GHz to 1.5 GHz.

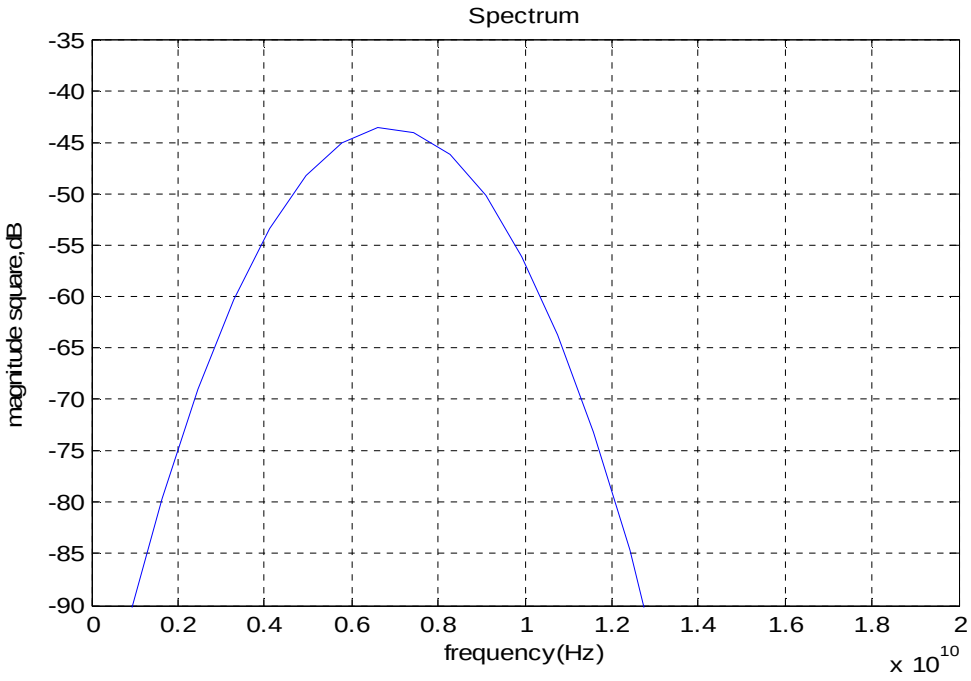

Figure 2.2.4, sampling frequency f_s = 50 GHz

Compared with narrow band and wide band signals, the UWB pulse spreads its energy thinly over a wide range from near d.c. to a few gigahertz. We can see in figure 2.2.5, that the bandwidth of UWB system is very broad and the energy of UWB is spread very thin, resulting in lower power consumption than other systems.

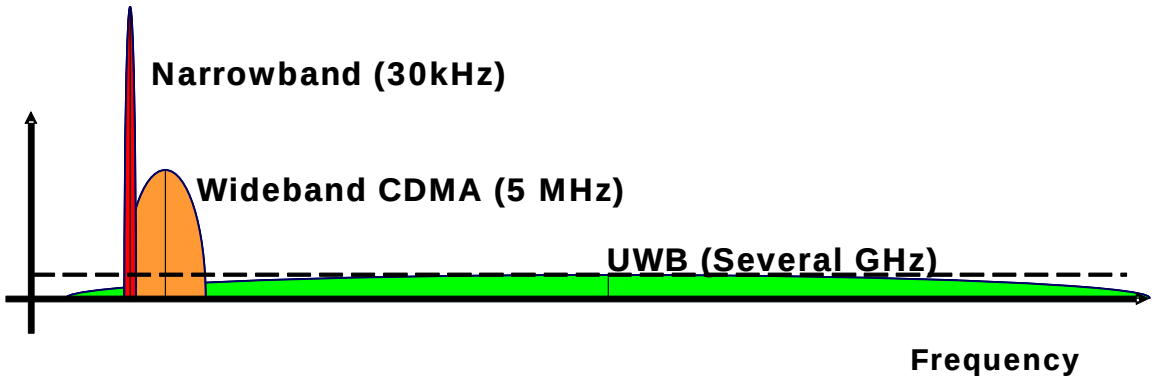

Figure2.2.5 UWB vs. other radio system

Due to such a broad range, interference by narrow band radio systems coexisting in the same bandwidth is common. To mitigate the effects of this interference, spread spectrum techniques may be used. DSSS and time-hopping spread spectrum are the most popular techniques. Both of them are used generally for UWB radio system. However, DSSS will not be discussed here. Since only a single user environment will be considered in the ensuing chapters.

3. Modulation Type

Before a binary data stream is transmitted through a communication channel, we utilize a type of pulse modulation process, which produces a signal that can be easily accommodated by the channel. In pulse modulation, either the amplitude or position or width of the pulse will vary on one-to-one basis with the binary ”1” or the binary ” 0”. Three types of modulations are briefly described in this chapter: On-off keying (OOK), Pulse amplitude modulation (PAM), and Pulse position modulation (PPM). They are all widely used by modern UWB systems.

3.1 OOK

OOK is a simple form of pulse amplitude modulation technique. The pulse is transmitted when a binary 1 is sent while no pulse is transmitted to indicate that a binary 0 is sent. This modulation was traditionally used to transmit Morse code over a radio frequency and is illustrated in Figure 3.1.1

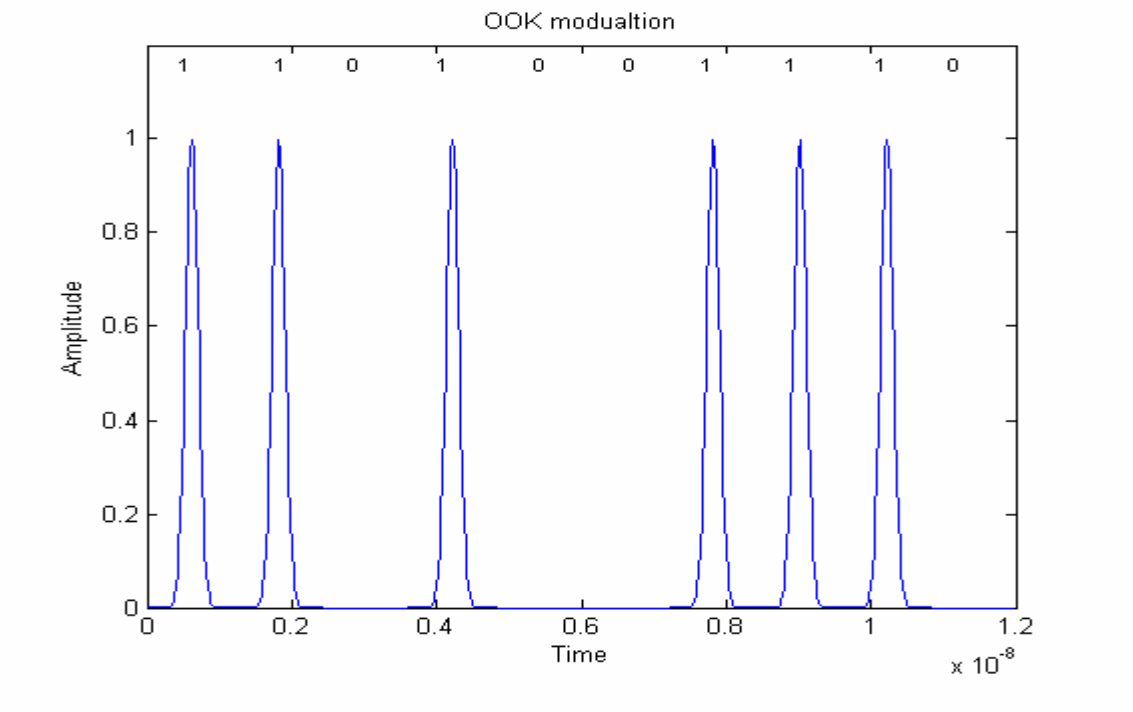

Figure 3.1.1 On-Off Keying

The OOK modulation is described as follow [12]:

$$p(t) = \sum_{j=-\infty}^{\infty} b_j s(t - jT_f) \tag{3.1.1}$$

Where, $p(t)$ is a pulse train
$b_j \in \{0,1\}$ is a binary information symbol
$s(t)$ is the transmitted pulse waveform
T_f is the pulse repetition time

The benefit of using an OOK modulation is the simplicity of its implementation. As seen in the equation 3.1.1, we only need a binary generator combined with a pulse generator. There is no need for the use of sophisticated physical components. Although OOK can reduce the complexity for the UWB system, it has several drawbacks.

First of all, we are to likely lose synchronization at the receiver if the transmitted data includes a steady stream of zeros. Second, the difference in pulse amplitude may be small, its immunity against noise is reduced. Third, when compared with binary PAM, OOK modulation has lower BER performance. The decision process is more accurate when the gap between maximum and minimum amplitude is larger. For OOK modulation, the gap is twice as small as binary PAM modulation. This is clearly shown in figure 3.1.2, where bit errors occur much more often when OOK modulation is applied.

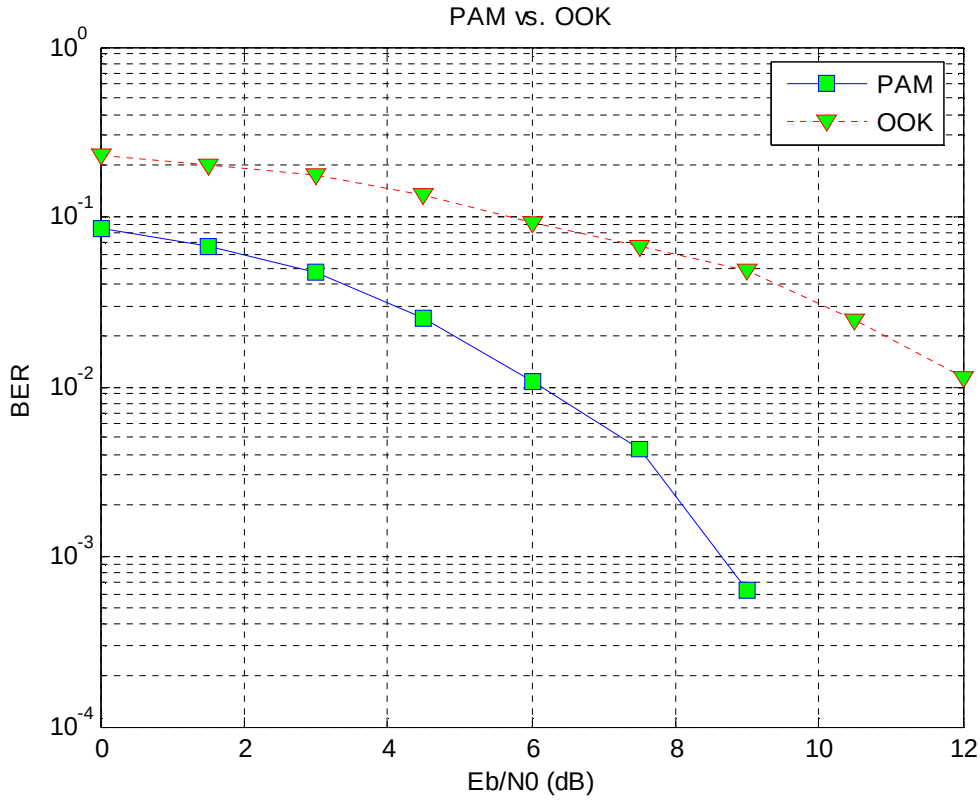

Figure 3.1.2 BER for OOK and BPSK

3.2 PAM Modulation

Bipolar PAM is also a simple digital modulation method. In this type of modulation, the information is conveyed by adjusting the amplitude of the transmitted signal. In PAM, the information data bit "1" is represented by a pulse of amplitude A while the information data bit "0" is represented by a pulse of amplitude –A. Binary PAM is illustrated in Figure 3.2.1. The mathematical representation of Binary PAM is given as [12]:

$$p(t) = \sum_{j=-\infty}^{\infty} b_j s(t - jT_f) \qquad (3.1.2)$$

where, $p(t)$ is an UWB pulse train

$b_j \in \{-1,1\}$	is the binary information symbol
$s(t)$	is transmitted pulse waveform
T_f	is the pulse repetition time

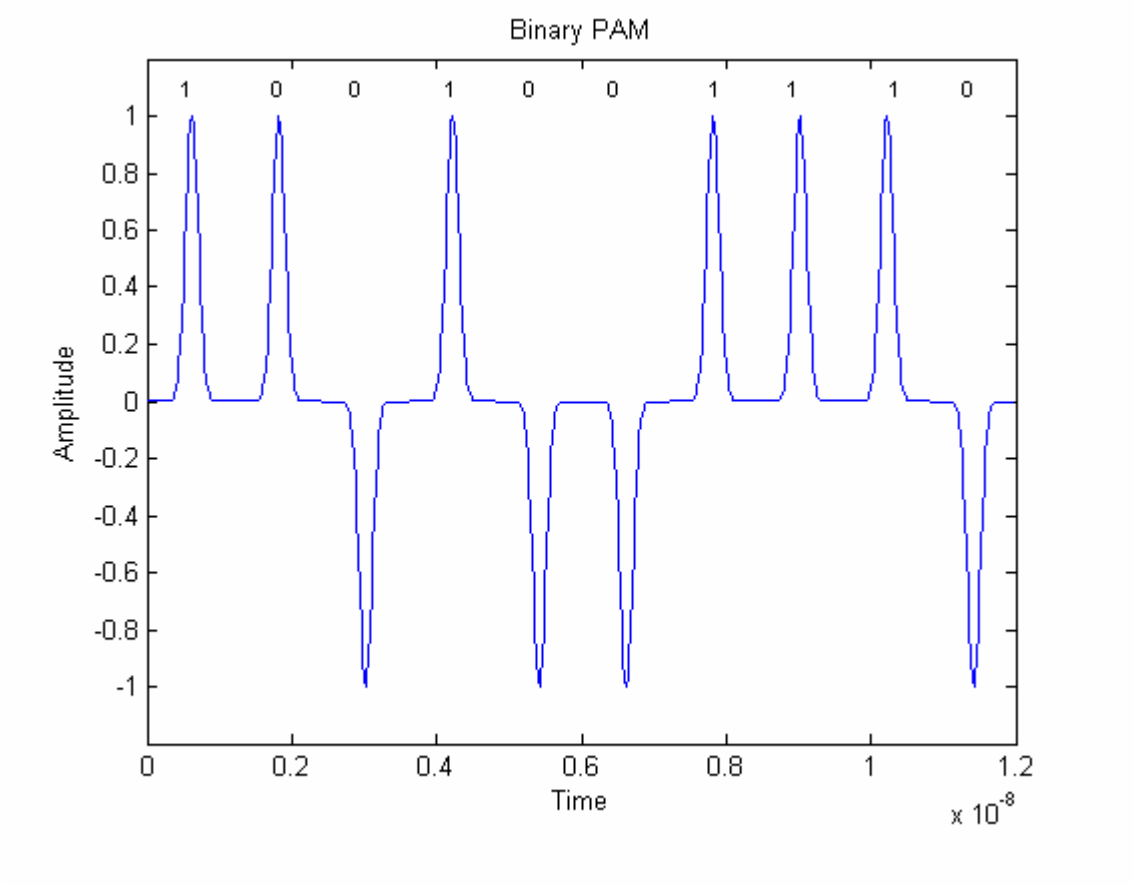

Figure 3.2.1 Binary PAM

The advantage of bipolar PAM modulation is its improvement of BER performance. The increased performance occurs because the pulse amplitude for bipolar PAM is twice as large as the pulse amplitude for OOK.

Unfortunately, there are some drawbacks in using a binary PAM modulation such as complex implantation and non-periodicity. The complexity of physical implementation is increased due to polarity pulse. While using OOK modulation, only one pulse generator is needed as compared to two or more pulse generators for Binary PAM modulation.

3.3 PPM

A PPM signal consists of a stream of pulses where the pulse displacement from a specified time reference is proportional to the sample value of information data. Generally, a pulse is transmitted at the time position of prototype pulse as a binary "1" is sent; likewise, a pulse transmitted with additional delay for binary "0".Figure 3.3.1 illustrates a PPM modulation.

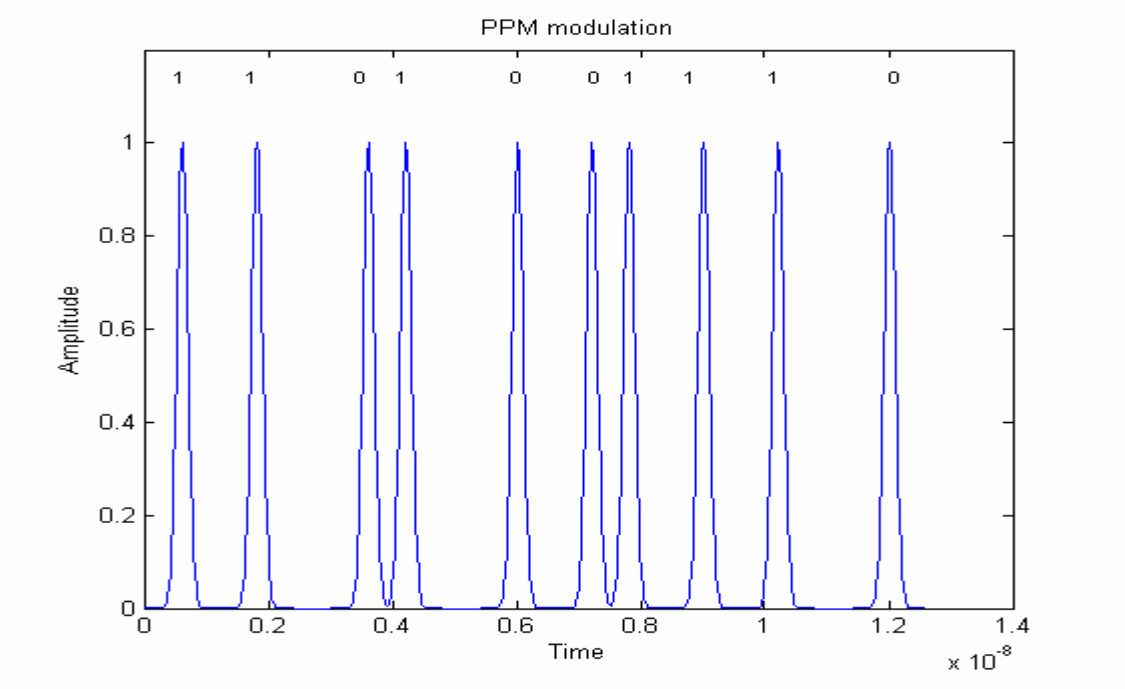

Figure 3.3.1 PPM

PPM modulation can be expressed by [12]:

$$p(t) = \sum_{j=\infty}^{\infty} s(t - jT_f - db_j) \tag{3.1.3}$$

where, $p(t)$ is an UWB pulse train
$b_j \in \{0,1\}$ is a binary information symbol
$s(t)$ is transmitted pulse waveform
T_f is the pulse repetition time
δ is the modulation index (time delay)

The primary advantage of PPM is that it can be implemented non-coherently, as the phase lock loop is unnecessary for tracking the carrier phase. The PPM modulation is particularly beneficial to optical communication systems where coherent modulation and detection costs are prohibitively high.

One of the disadvantages of PPM is its sensitivity to multipath interference that arises in channels with selective frequency fading. In multipath environments, the received signals are always composed of one or more transmitted pulses. It is difficult to extract the information from these received signals since the information is encoded at the time of arrival. Aside from its susceptibility to multipath interference, another drawback of PPM modulation is that it may suffer from synchronization loss. As the pulse stream is transmitted the receiver measures the timing of each arriving pulse, if the detection scheme is not able to synchronize with local time, the meaning of the symbol will be unrecognizable.

3.4 Conclusion

Three types of pulse modulations, along with their particular advantages and disadvantages have been briefly discussed here. For example, in the case of OOK modulation, it is easily implemented but a poor BER performer. Due to its simplicity and overall better BER performance, Binary PAM will be used in this thesis.

4. Proposed System Design

In this chapter, we will present the design of the proposed system. First the transmitter architecture will be described, followed by a discussion of the channel model. Then the receiver implementation strategy will be elaborated on.

4.1 Transmitter Architecture

As pointed out in chapter 3, due to its simplicity, Binary PAM modulation is used in this thesis. Binary PAM modulation can be implemented by generating a stream of random binary bits and passing through the pulse shape filter described. Prior to pulse shaping, a simple convolutinal encoder is used to achieve a better BER performance. Our transmitter architecture is illustrated in the figure 4.1.1:

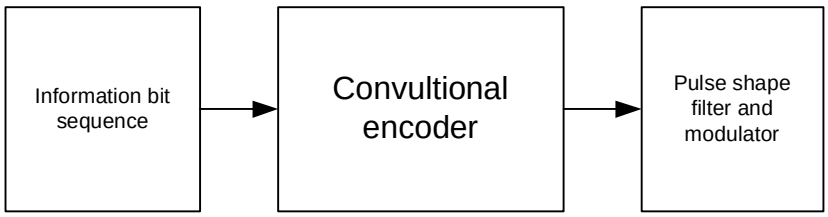

Figure 4.1.1 transmitter architecture

4.1.1 Convolutional codes

In order to increase reliability and improved BER performance, a simple convolutional encoder is used. Specifically, we use a constraint length v = 5 and code rate R = ½ convolutional encoder [9]. Figure 4.1.2 illustrates the block diagram of convolutional encoder with generator polynomial g(x) = (23, 35) and free distance d_f = 7. Figure 4.1.3 shows the trellis generated by the code.

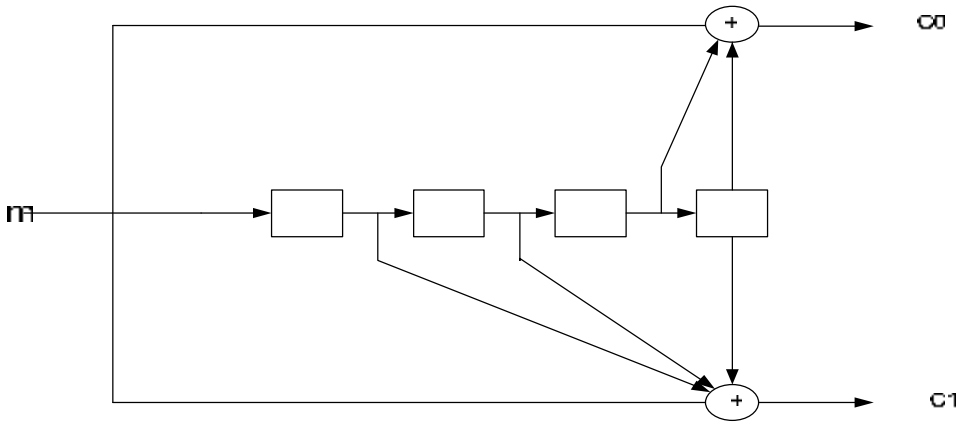

Figure 4.1.2 Rate ½, M = 4 convolutional encoder

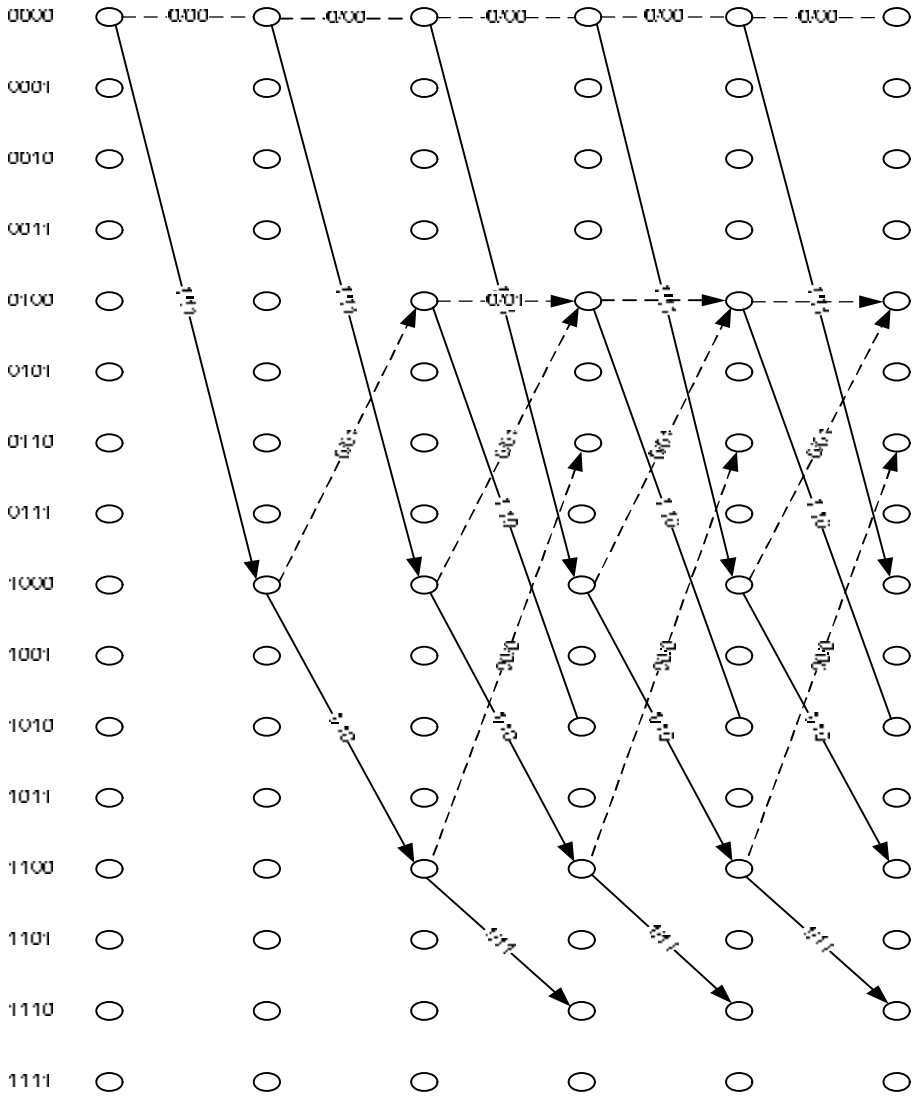

Figure 4.1.3 trellis diagram

4.1.2 Viterbi Decoding

As is well known, there are two types of decoding strategies "*Hard-Decision decoding*" and "*Soft-Decision decoding*" . Hard-Decision decoding has a simple implementation even though soft-decision decoding has a better BER performance. Figure 4.14 shows the difference in performance between the two decision strategies when transmission occurs over an AWGN channel.

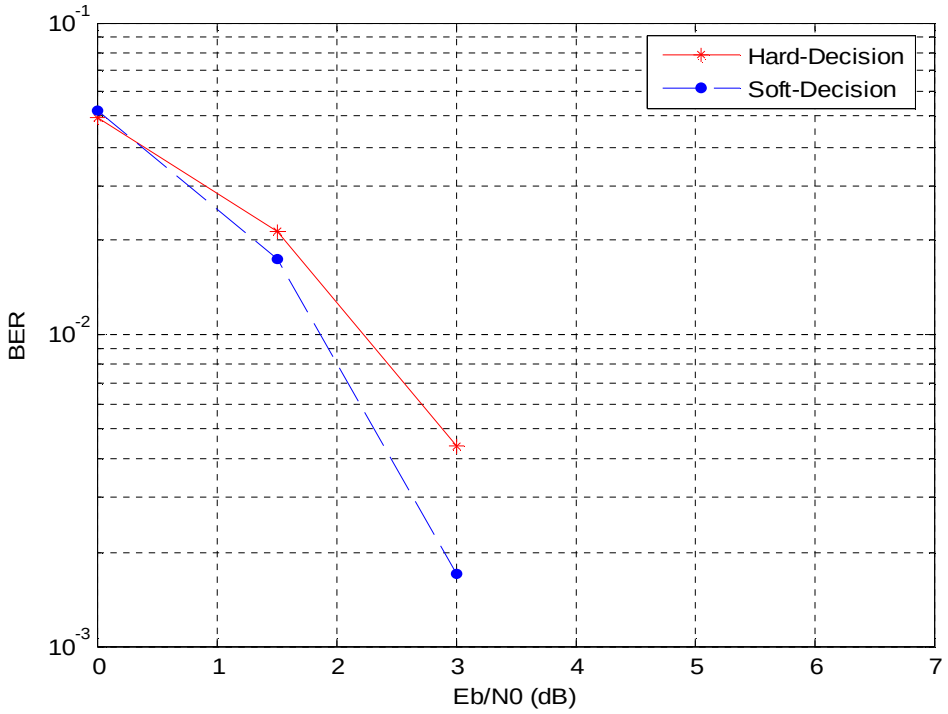

Figure 4.1.4 Comparison of soft/hard decision

4.2 Channel Model

The transmitted signal propagates through the channel and white Gaussian noise (WGN) is added at the detector. Hence, the resulting signal is corrupted by noise and channel distortion. In this section, the characteristics of channel are discussed in the context of a multipath environment. Multipath occurs when the transmitted signal arrives at the receiver via multiple propagation paths. Consequently, the received signal suffers from undesired effects such as fading problem, Inter-Symbol

Interference (ISI) and other types of distortion. Those are caused by the phase, attenuation, delay and Doppler shift of each path.

4.2.1 Band-limited Channel

Unlike the additive Gaussian noise channel, many communication channels have a constraint on bandwidth. This sort of channel could be generally characterized as band-limited linear filter with bandwidth of *W* Hz. It also has an equivalent low-pass frequency response C (*f*), which is expressed as [11][14]:

$$C(f) = A(f)e^{jq(f)} \qquad \text{, C } (f) = 0 \text{ for } |f| > W,$$

where A (*f*),$q(f)$ are the amplitude and the phase responses, respectively. We also define the group delay as:

$$t(f) = -\frac{1}{2p}\frac{dq(f)}{df} .$$

Sometimes group delay is used to replace phase response.

When the amplitude response stays constant and the phase response is a linear function of frequency within the bandwidth *W*, we can say that the channel is ideal. In the case when A (*f*) is not a constant or $q(f)$ is no longer a linear function of frequency response within bandwidth *W*, the channel is not ideal anymore. The signal transmission at a symbol rate which is equal or exceeding *W* results in interference among a number of adjacent symbols. Figure 4.2.1 illustrates the frequency response of band-limited channel and the frequency response of Gaussian pulse, both of which are used for simulations. As seen below, the bandwidth of Gaussian pulse exceeds *W* (channel bandwidth). The distortion is as expected.

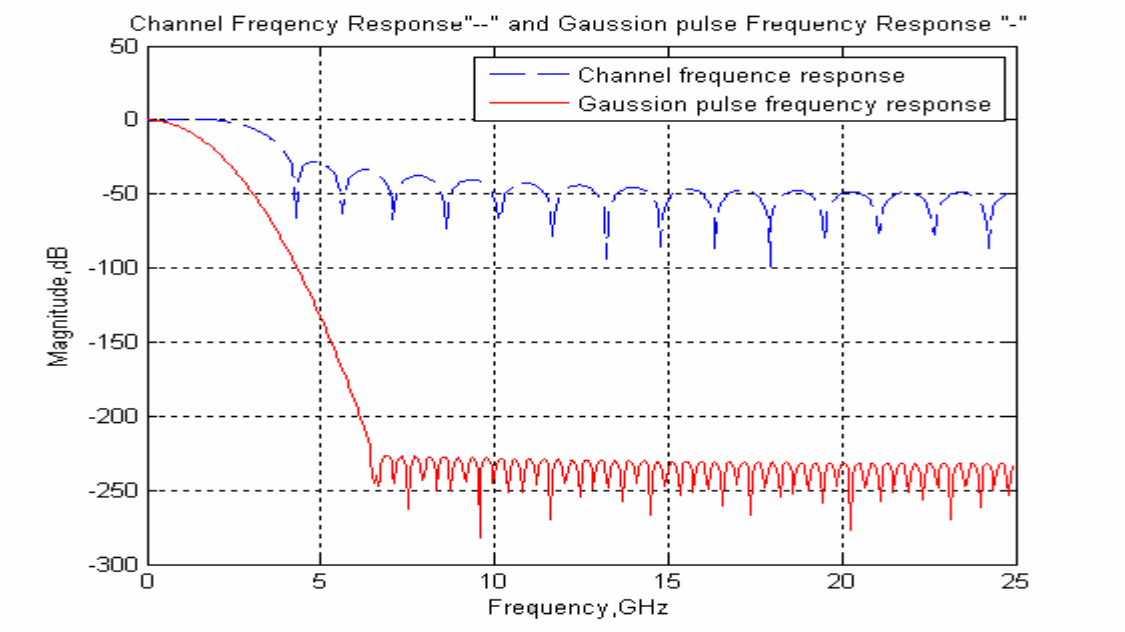

Figure 4.2.1 Channel Frequency response

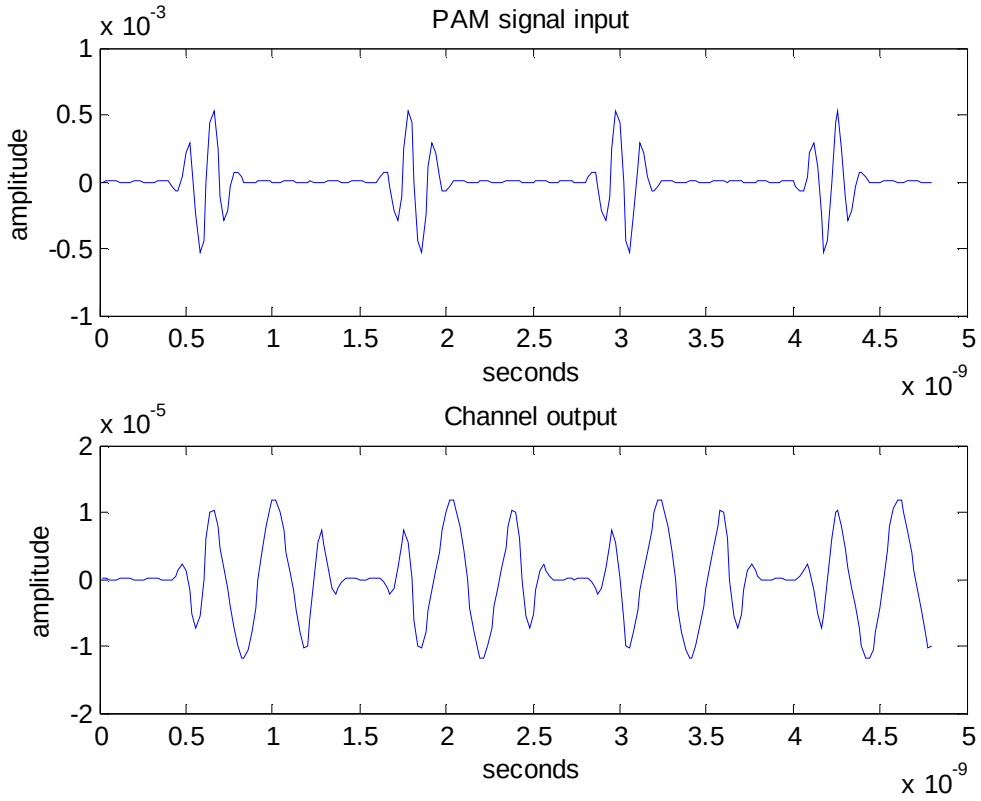

Figure 4.2.2 Effect of channel distortion

Figure 4.2.2 shows the distortion caused by the band-limited channel. The upper part illustrates when the UWB pulse train is transmitted through an ideal channel. The bottom part reflects the effect of channel distortion. The transmitted pulse sequence is no longer easily distinguishable. This effect can be compensated by applying an equalizer at demodulator.

4.2.2 Multipath Channel

For signal transmission, there always exist more than one propagation path from transmitter to receiver. In an indoor environment, those paths are caused by reflections from both stationary and moving objects. As a consequence, the transmitted signal arrives at the receiver via different propagation paths associated with time delays. Such a channel is of the time-varying type which can be characterized by a linear filter with time-variant impulse response.

Due to this time variant property, the response of the channel will vary with time. Therefore, if we transmit an extremely short pulse through the channel and then repeat this experiment over again, we shall observe changes in the received pulse train, such as changes in the number of individual pulse shape, changes in the number of pulse train, changes in the relatively delays among each pulse and so on. The channel response becomes unpredictable. For this reason, we need to characterize the time-variant multipath channel statistically.

Consider the transmission of an unmodulated carrier at frequency f_c, which can be expressed as:

$$C = A\cos 2pf_c t \tag{4.2.1}$$

Assuming that multiple path propagation occurs, each path is associated with a propagation delay and an attenuation factor. Because of the time variant structure of the medium, the propagation delay and attenuation factor also vary with time. In this case, the received signal may be described mathematically as follows:

$$X(t) = A\sum_n a_n(t)\cos[2pf_c(t - t_n(t))] \quad (4.2.2)$$

$$= A\mathrm{Re}\left\{\sum_n a_n(t)e^{-j2pf_c t_n(t)}e^{j2pf_c t}\right\} \quad (4.2.3)$$

where, a_n (t) is the attenuation factor and $t_n(t)$ is the propagation delay relative to each path.

From equation 4.2.3, we can obtain the representation of the equivalent low-pass channel which is expressed as:

$$C_l(t) = \sum_n a_n(t)e^{-j2p\, f_c t_n(t)}$$
$$= \sum_n a_n(t)e^{-jf_n(t)} \quad (4.2.4)$$

The time-variant phase term $f_n(t)$ in equation 4.2.4 results in signal fading. When signal fading takes place, the amplitude of the received signal varies with time. A number of fading channels have been studied. The characteristic of a fading channel is determined by the probability distribution of the channel impulse response such as Rayleigh or Ricean fading channel.

4.2.3 Channel Fading

As previously discussed, the amplitude of the received signal varies randomly with time. This phenomenon is called signal fading and determined by the time-varying phase term $f_n(t)$. There are several probability distributions modeling the statistical characteristics of the fading channel.

Rayleigh Fading

As the impulse response of channel is modeled as a zero-mean complex-valued Gaussian process, the envelope of impulse response at any time *t* is Rayleigh distributed. We call such channel Rayleigh fading channel.

Ricean Fading

Because of fixed scatterers or signal reflectors in the transmission medium, in addition to randomly moving scatterers, the impulse response of channel can no longer be modeled as having zero-mean. In this case, the envelope of channel impulse response has a Ricean distribution. Thus, such channel is called Ricean fading channel.

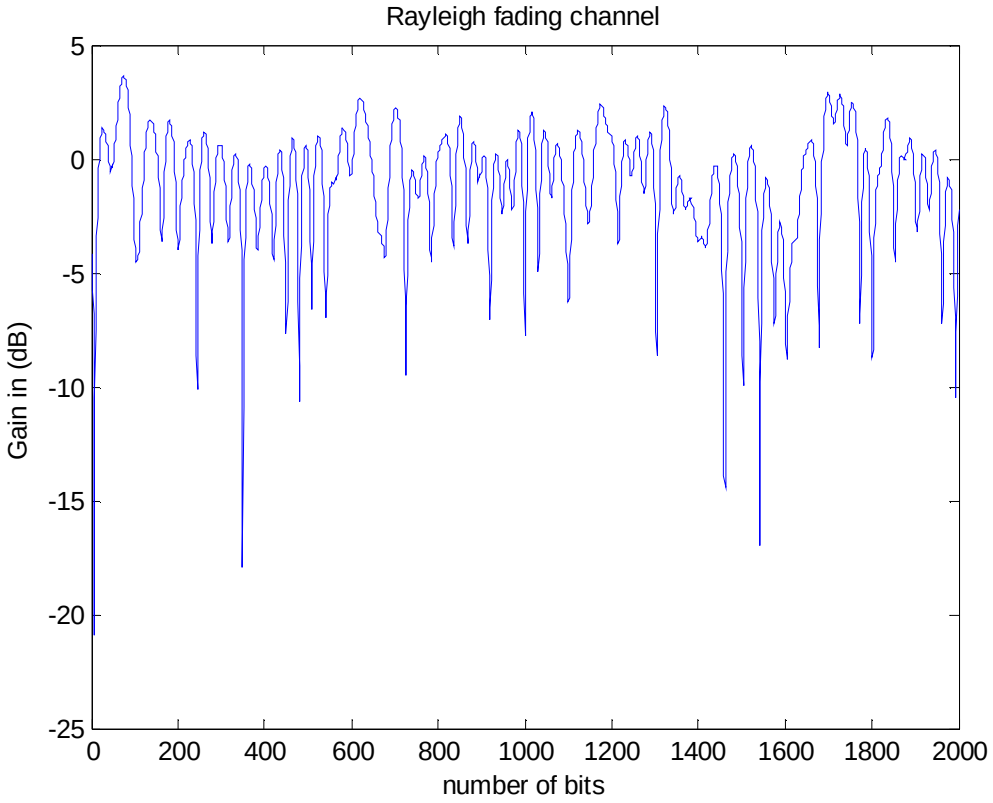

Figure 4.2.3 Rayleigh fading channel

Figure 4.2.3 shows the simulation of a Rayleigh fading channel.

4.3 Receiver Design

The receiver design is now discussed. The basic theory of filter banks is presented. Due to the very wide bandwidth of UWB system, it is hard if not impossible to design high speed ADCs with today's technology. This problem can be solved if the received UWB signal is split into a number of subbands by power

splitters, analog low-pass filters, mixers and digital filters [1]. Each of subbands is sampled at a fraction of effective sampling frequency. Figure 4.3.1 (a) and (b) show the block diagram of the receiver implementation. The complexity is relaxed and efficiency is enhanced. At the synthesis part of receiver, it is preferable to estimate optimally the transmitted signal rather than reconstruct it perfectly. Adaptive filters performing minimum mean square error criterion are employed as synthesis filter. At the output of receiver, the estimated signal is input to a decision device. A comparator is used to make decisions to regenerate the transmitted sequence before channel decoding.

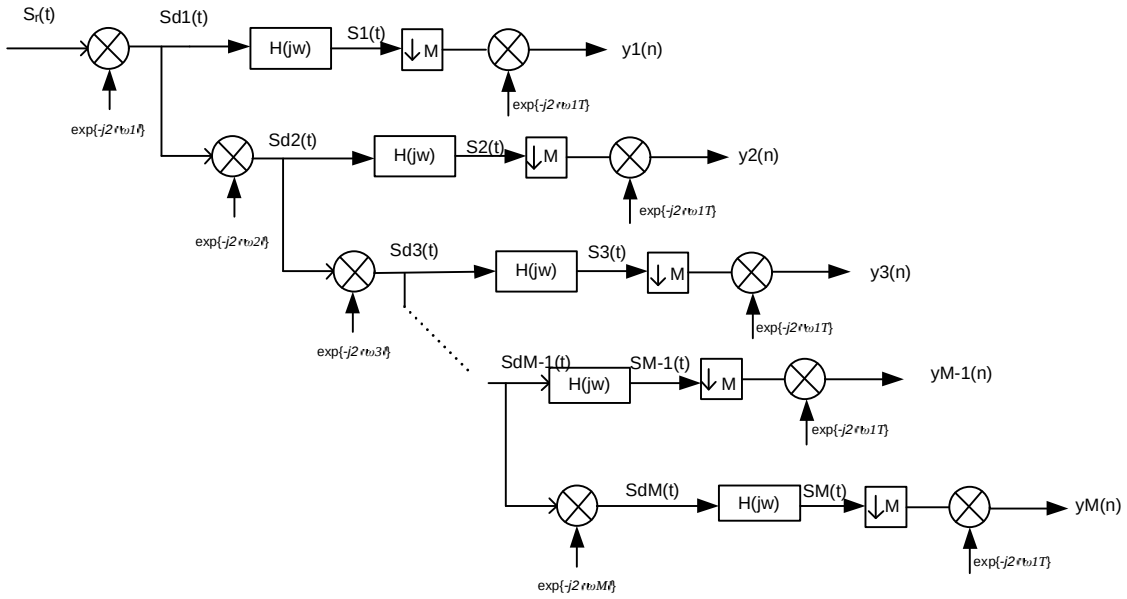

(a)

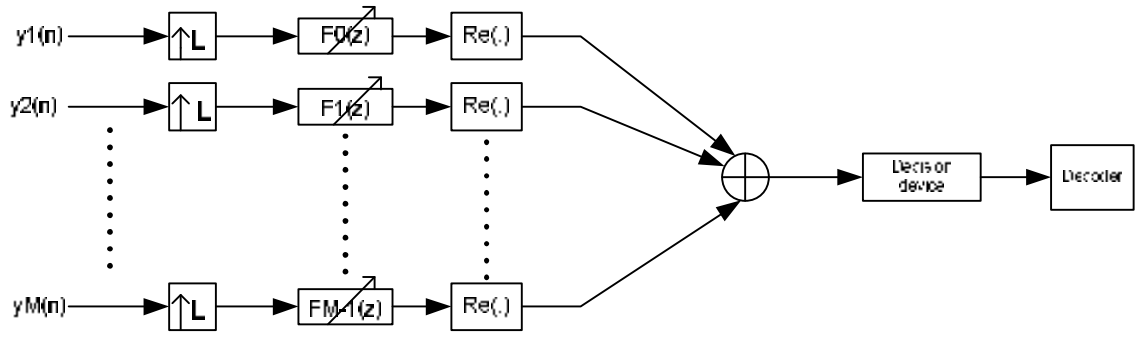

(b)

Figure 4.3.1 (a) analysis and (b) synthesis filter bank

4.3.1 Digital Filter Bank

Let us briefly discuss the fundamentals of digital filter banks.

The M-fold Decimator:

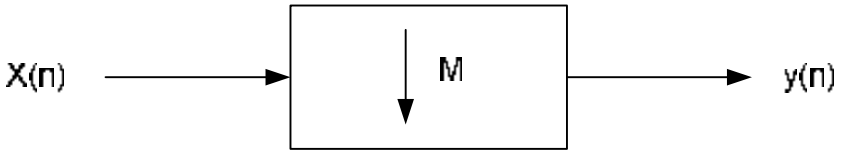

Figure 4.3.2 Illustration of an M-fold decimator

Figure 4.3.2 shows the block diagram of an M-fold decimator. Its function is to downsample the input signal at rate, (1/M)th of input sequence. Consequently, it might cause loss of information. We can express the M fold decimator mathematically [13]:

$$y(n) = \begin{cases} x(n), n = 0, \pm M, \pm 2M, \ldots \\ 0 \quad , otherwize \end{cases} \tag{4.3.1}$$

where, M is an integer. The samples of y(n) result from the samples of x(n) occurring only at time equal to multiples of M.

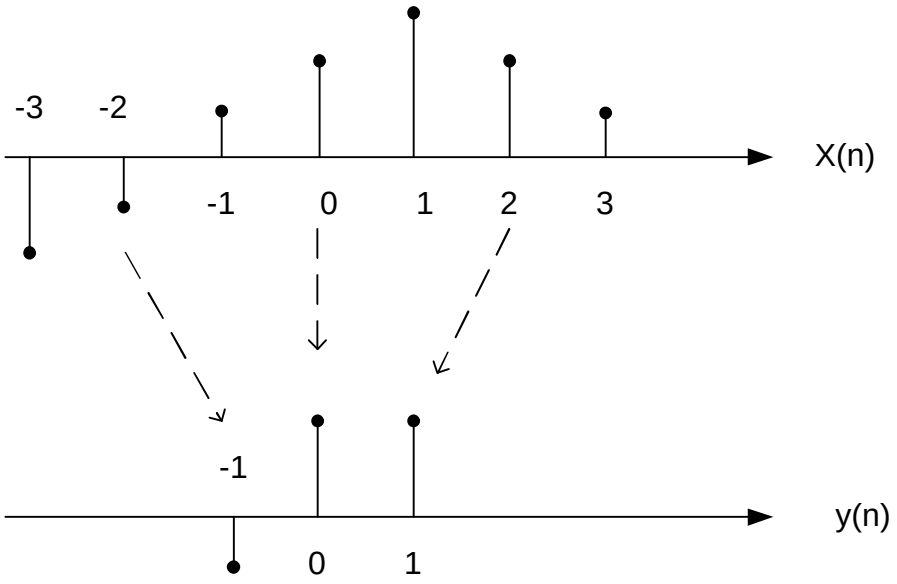

Figure 4.3.3 Illustration of a decimator

The L-fold Interpolator:

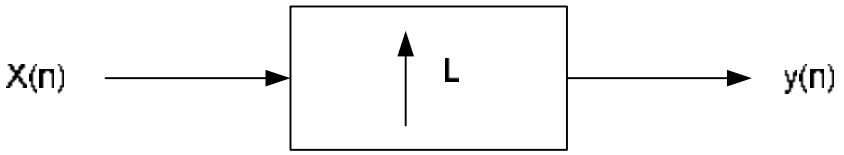

Figure 4.3.4 Illustration of a L-fold interpolator

Figure 4.3.3 shows the block diagram of a L-fold interpolator. Its purpose is to up-sample the input signal x(n) at rate L times larger than input sequence. The mathematical representation of interpolator can be expressed as [13]:

$$y(n) = \begin{cases} x(n/L), n = 0, \pm L, \pm 2L, \mathbf{L} \\ 0 \qquad otherwise \end{cases} \tag{4.3.2}$$

where, L is a positive integer, this operation is implemented by appending L-1 equidistant zero-valued samples between two consecutive samples of the input sequence. Figure 4.3.5 shows the illustration of a L-fold interpolator for L=3

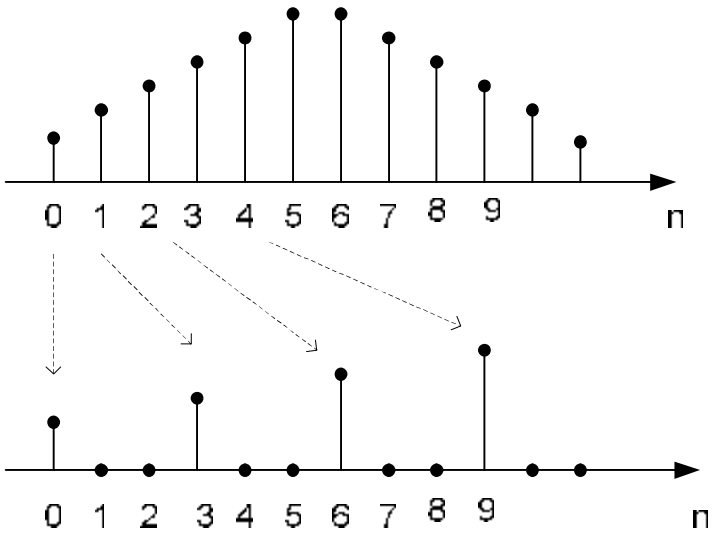

Figure 4.3.5 3-fold interpolation

Filter Bank

When we assemble a number of filters, those filters have a common input or a common output. We can call a collection of filters a “filter bank”. It includes the analysis part and synthesis part. In the analysis part, the signal is split into several subbands. Each subband is sampled at the fraction of sampling frequency. The output of the analysis filter bank is followed by a synthesis filter bank which reconstructs the desired signal from amplitude distortion, phase distortion and aliasing distortion. A number of works have been studied to perfectly reconstruct the transmitted signal.

In this thesis, we focus on a hybrid filter bank (HFB). Continuous-time analog analysis filters and discrete-time synthesis filters are employed. Such filter bank is called hybrid filter bank. Elimination of the distortion caused by the multipath propagation is the main goal of the HFB design. As stated before, the transmitted signal is not reconstructed perfectly by the synthesis filter banks. Instead, the information and data are collected from each branch of the system and then the transmitted signals for data detection are estimated in an optimal fashion. By using an adaptive synthesis filter, we optimally estimate the transmitted signal. The synthesis filters here perform a combination of match filtering, channel estimation and aliasing cancellation.

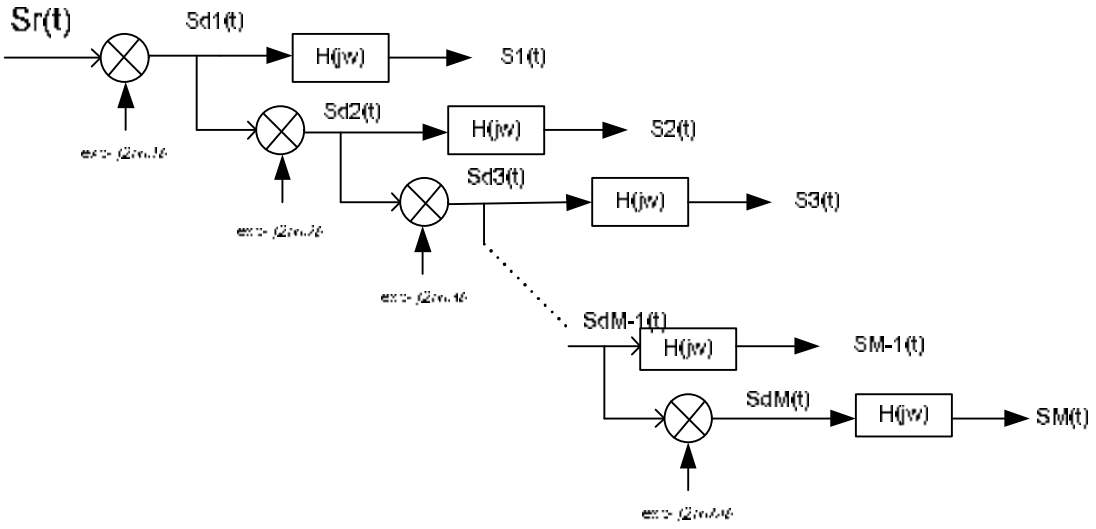

Figure 4.3.6 Front-end filter bank architecture

Figure 4.3.6 shows a block diagram of the front-end filter bank. By using mixers and low-pass filters, M subband signals are obtain at the output. In this implementation, H(jw) is an analog LPF, $S_i(t), i = 1,...,M$ are the subband signals, $w_i = 1,...,M$ is the frequency of operation of the complex mixer in rad/s. Assuming the UWB signal is an input of presented architecture, the resulting outputs are shown in the following figures:

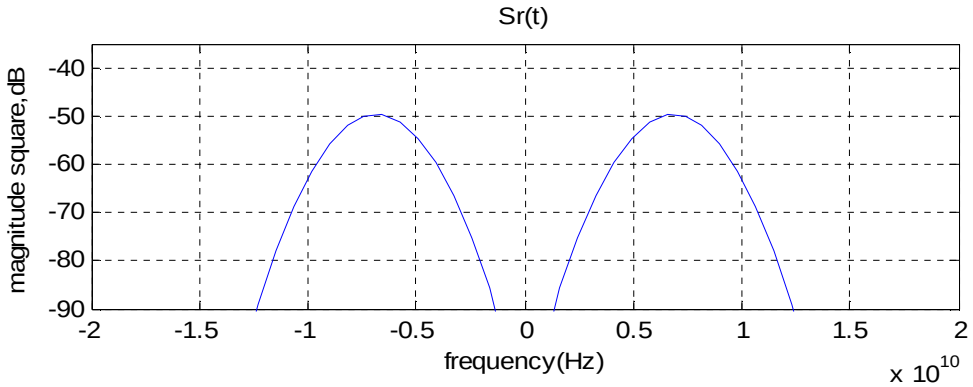

Figure 4.3.7 the magnitude response of received signal $S_r(t)$

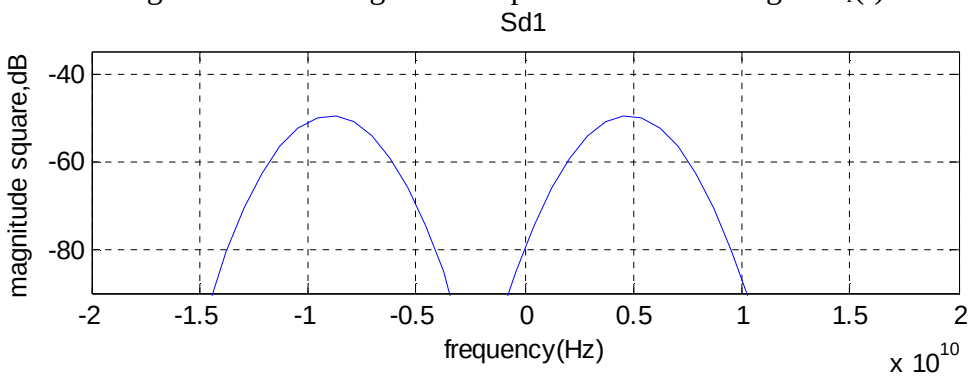

(a)

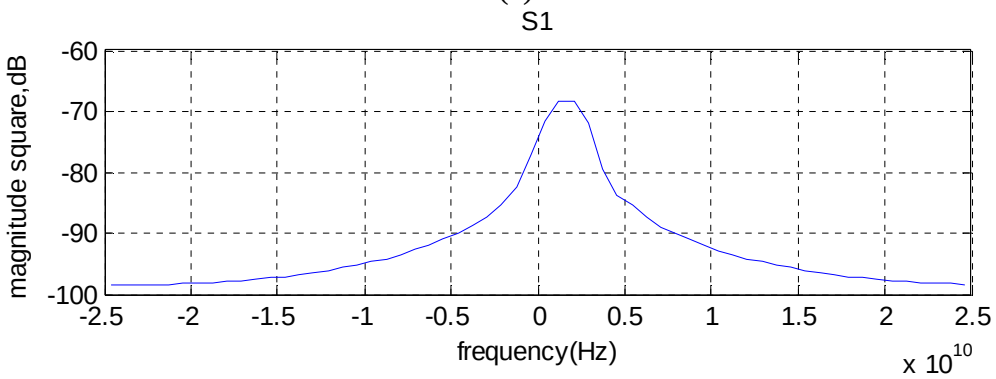

(b)

Figure 4.3.8(a) spectrum of S_{d1}(b) spectrum of S1

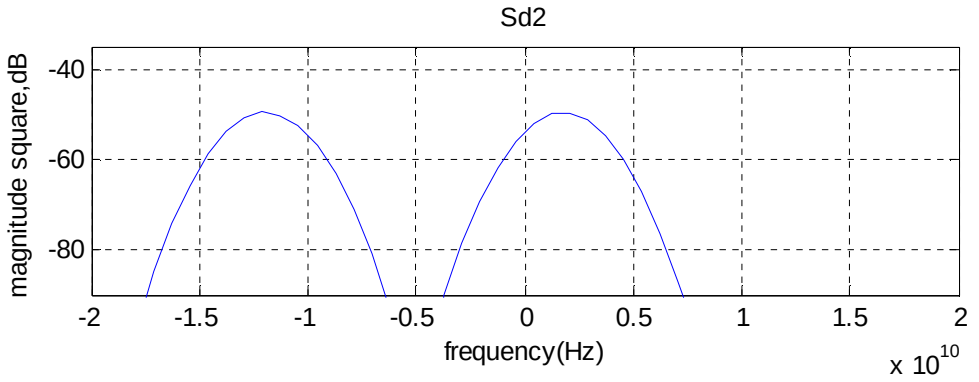

(a)

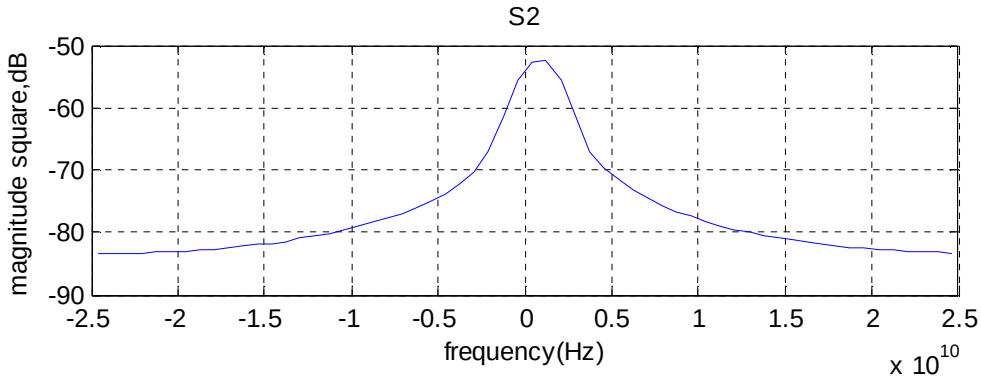

(b)

Figure 4.3.9 (a) spectrum of S_{d2} (b) spectrum of S2

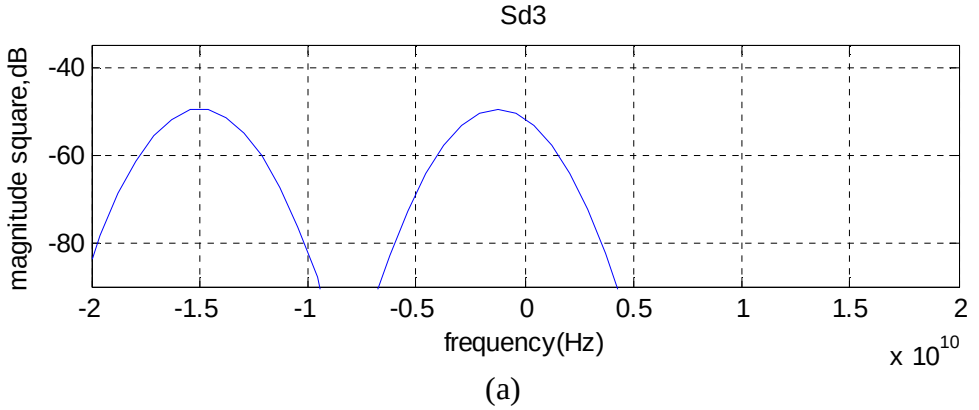

(a)

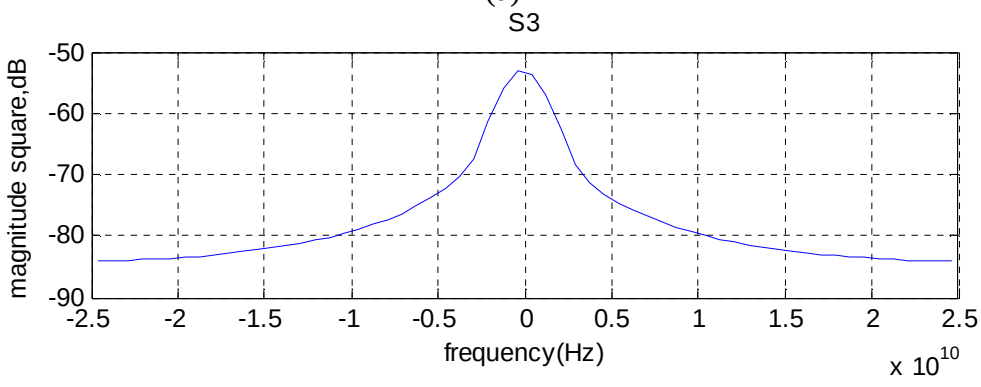

(b)

Figure 4.3.10 (a) spectrum of S_{d3} (b) spectrum of S3

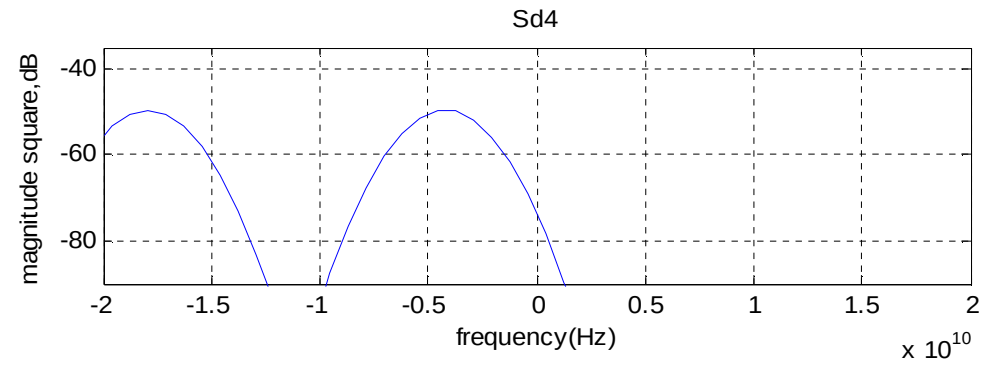

(a)

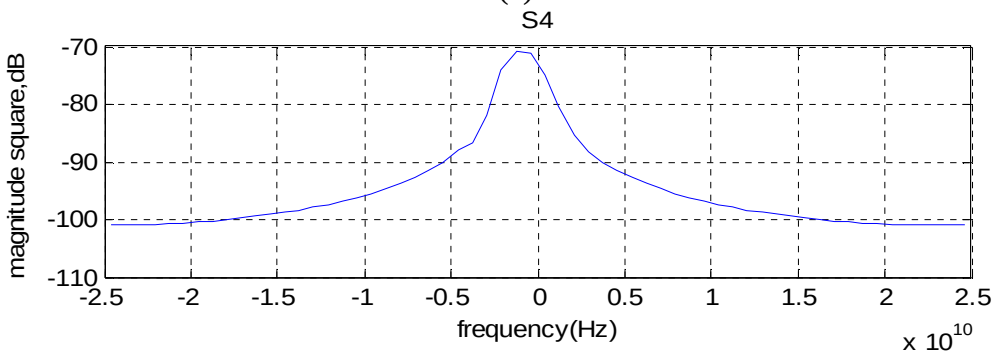

(b)

Figure 4.3.11 (a) spectrum of S_{d4} (b) spectrum of S4

The figure 4.3.7-4.3.11 show the magnitude responses of an UWB signal and subband signals obtained from the outputs of a front-end filter bank. Instead of using a band-pass filter bank, the mixers and low-pass filters are used to relax the implementation requirement. The signal $S_{d1}(t)$ (shown in the upper side of figure 4.3.8) is obtained by down-converting the received signal (shown in the figure 4.3.7) to baseband by using a mixer. Also, the $S_{di}(t)$, i=2,3,...are obtained by shifting $S_{di-1}(t)$ to left in the frequency axis. As down-converted signals are filtered by low-pass filters, the different frequency segments of received signal can be extracted. The lower sides of figure 4.3.8-4.3.11 illustrate the subband signals $S_i(t)$, i=1,2,…

4.3.2 Adaptive Filter

Again instead of perfectly reconstructing the transmitted signals, the synthesis filters are designed to optimally estimate the transmitted signal. Thus, the synthesis filters can be implemented by using linear adaptive filters. Such filters perform minimum mean-square error (MMSE) estimation. The coefficients of the adaptive filters are adjusted in order to minimize the mean square error which can be expressed as $MSE = E\{|e(n)|^2\}$.

A number of algorithms have been used to minimize mean square error. Here we consider two types of adaptive filters using Wiener-Hopf filter and the filter based on the Least-Mean-Square (LMS) algorithm [14][16].

Wiener Filter

Let y(n) and d(n) denote a desired signal and an output estimate respectively, given a set of inputs $\{u(i) : i = 0,1,2,3.....\}$ ɜ the mean-square value of the estimation error $e(n) = d(n) - y(n)$ is minimized. The output of the filter is defined by:

$$y(n) = \sum_{k=0}^{\infty} w_k u(n-k), n = 0,1,... \tag{4.3.3}$$

where, the w_k's are assumed to be complex-valued.

The objective is to minimize the MSE criterion

$$J = E\{|e(n)|\}, \tag{4.3.4}$$

$$\text{i.e. , } \nabla_k J = -2E\{u(n-k)e^*(n)\} = 0 \tag{4.3.5}$$

equivalently, $$E\{u(n-k)e_o^*(n)\} = 0, k = 0,1,... \tag{4.3.7}$$

where, $e_o^*(n)$ is the value that optimizes J and $\nabla_k J$.

Substituting $e(n) = d(n) - y(n)$ into the equation 4.3.7, yields:

$$E\{u(n-k)[d^*(n) - \sum_{i=0}^{\infty} w_{oi} u^*(n-i)]\} = 0, k = 0,1,... \tag{4.3.8}$$

where, w_{oi} is the ith coefficient of the impulse response of the optimum filter.

Performing the expectation explicitly, we can get :

$$E\{u(n-k)d^*(n)\} = \sum_{i=0}^{\infty} w_{oi} E\{u(n-k)u^*(n-i)\}, k = 0,1,... \qquad (4.3.9)$$

Let u(n) and d(n) be WSS random processes, the equation (4.3.9) can be described as:

$$\sum_{i=0}^{\infty} w_{oi} r(i-k) = p(-k), k = 0,1,... \qquad (4.3.10)$$

where, $r(i-k) = E\{u(n-k)u^*(n-k)\}$ the auto-correlation of input signal, $p(-k) = E\{u(n-k)d^*(n)\}$ the cross-correlation between the input signal and the desired signal.

This equation is known as the Wiener-Hopf equation. In the practice, the order of filter is not infinite. For an M taps adaptive filter, assuming we have an input vector which is defined as: $\underline{U}(n) = [u(n), u(n-1), ..., u(n-(M-1))]^T$ and coefficient weight vector $\underline{w}_o = [w_{o,1}, w_{o2}, ... w_{o,M-2}]^T$, we also define the auto-correlation matrix $R = E\{\underline{u}(n)\underline{u}^H(n)\}$ and cross-correlation vector $\underline{p} = [p(0), p(1), ...p(-(M-1))]^T$

Consequently, equation 4.3.10 can be rewritten as:

$$R\underline{w}_o = \underline{p} \qquad (4.3.11)$$

Multiplying both sides of this equation by R^{-1}, the inverse of the auto-correlation matrix, we obtain

$$\underline{w}_o = R^{-1}\underline{p} \qquad (4.3.12)$$

where $\underline{w}_o$ is an optimum weight vector for the Wiener filter.

The auto-correlation matrix R is given by:

$$R = \begin{bmatrix} r(0) & r(1) & ..... & r(M-1) \\ r^*(1) & r(0) & ..... & r(M-2) \\ r^*(2) & r^*(1) & ..... & r(M-3) \\ \mathbb{M} & \mathbb{M} & \mathbf{O} & \mathbb{M} \\ r^*(M-1) & r^*(M-2) & ..... & r(0) \end{bmatrix} \qquad (4.3.13)$$

We considered the possibility of implementing the Wiener filter, however, the simulation results herein use a LMS adaptive filter due to its simplicity.

LMS Adaptive Filter

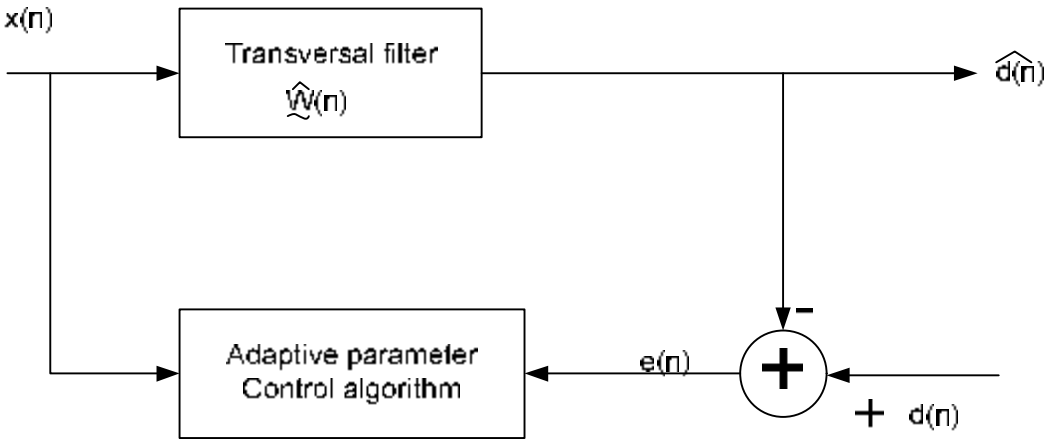

Figure 4.3.12 LMS adaptive filter block diagram

The block diagram shown in Figure 4.3.12 illustrates the LMS adaptive filter which can adapt the coefficient weight to minimize the least mean square of signal error. An estimate of the error is the difference between the desired response and the response based on input signal.

According to the method of steepest descent, the weight vector equation is given by:

$$\underset{\sim}{w}(n+1) = \underset{\sim}{w}(n) + \frac{1}{2}\mu\nabla J(n) \qquad (4.3.12)$$

where, μ is the step size parameter.

Because $\nabla J(n) = -2\underset{\sim}{p} + 2R\underset{\sim}{w}(n)$, which is substituted into equation 4.312.We obtain,

$$\underset{\sim}{w}(n+1) = \underset{\sim}{w}(n) + \mu[\underset{\sim}{p} - R\underset{\sim}{w}(n)] \qquad (4.3.13)$$

In this method, the challenge is the computation involved in finding the value of $\underset{\sim}{p}$ and R matrix in real time. Hence, the estimate of $\underset{\sim}{p}$, R and $\underset{\sim}{w}(n)$ are

used in equation 4.3.13 instead of actual value. The estimate of $\underline{p}$, R are expressed as:

$$\hat{R}(n) = \underline{u}(n)\underline{u}^{H}(n) \tag{4.3.14}$$

$$\hat{p}(n) = \underline{u}(n)d^{*}(n) \tag{4.3.15}$$

Equation 4.3.13 becomes

$$\underline{\hat{w}}(n+1) = \underline{w}(n) + m\underline{u}(n)[d^{*}(n) - \underline{u}^{H}(n)\underline{w}(n)] \tag{4.3.16}$$

$$\text{Or} \quad \underline{\hat{w}}(n+1) = \underline{w}(n) + m\underline{u}(n)e^{*}(n) \tag{4.3.17}$$

The LMS algorithm could be summarized in the following equations:

$$\text{Weight,} \quad \underline{\hat{w}}(n+1) = \underline{w}(n) + m\underline{u}(n)e^{*}(n) \tag{4.3.18}$$

$$\text{Error,} \quad e(n) = d(n) - y(n) \tag{4.3.19}$$

$$\text{Output,} \quad y(n) = \underline{\hat{w}}^{H}(n)\underline{u}(n) \tag{4.3.20}$$

The convergence is a considerable issue for LMS algorithm. If the step-size parameter, μ, is chosen to be very small, the algorithm converges very slowly. On the contrary, if μ is chosen to be large, it results in a faster convergence but it may lead to less stability. Thus, there exists a constraint on value of $\mu : 0 < m < \frac{2}{MS_{\max}}$, where S_{max} is the maximum value of the psd of the tap inputs *u(n)* and M is the number of filter tap coefficients.

In order to choose the value of μ appropriately, the number of filter tap coefficient M is fixed, and then different values of μ are applied. According to experiments, 0.25 is selected for μ when M is equal to 15.

5. Simulation Results

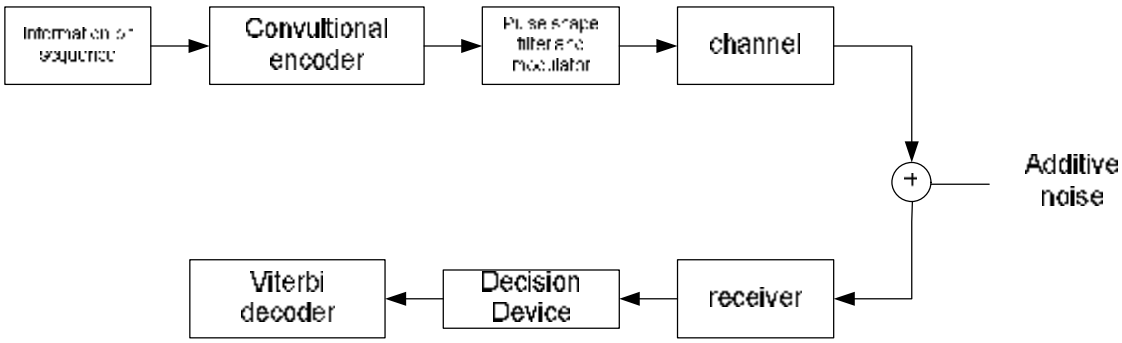

Figure 5.1 system architecture

In this chapter, simulation results that show the proposed system performance will be presented. To achieve this, a *Matlab* based simulation was implemented. Performance will be presented in the form of BER curves for different propagation environments such as single path, multipath with/without channel coding. The details of system simulation are specified: sampling rate f_s =50 GHz, carrier frequency 6.85 GHz.

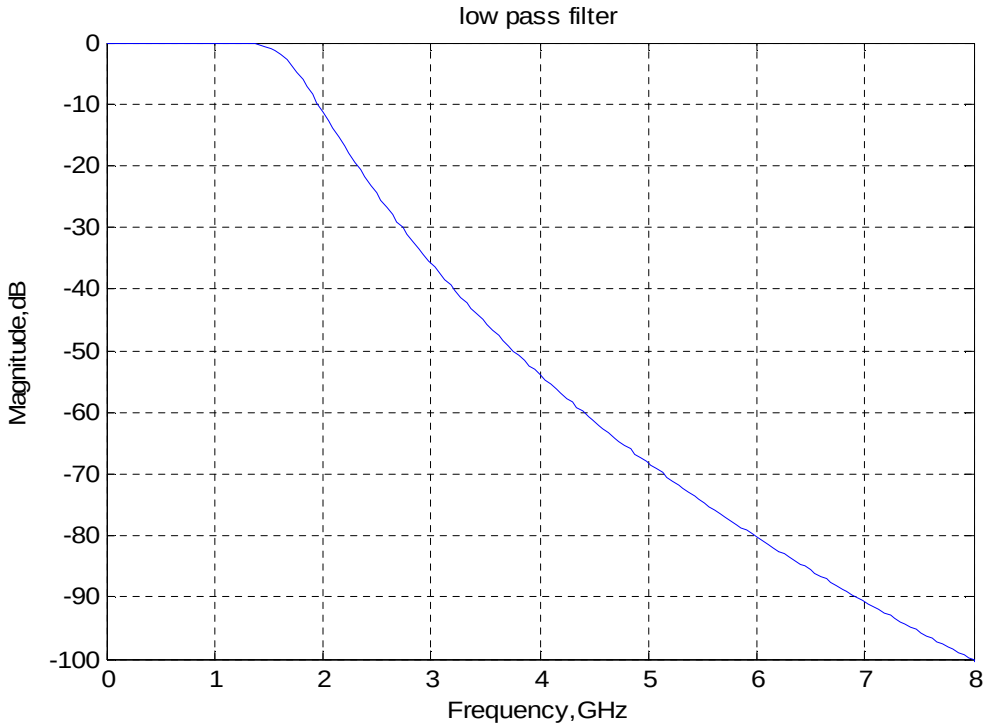

Figure 5.2 analog low pass filters

For the filter bank design, analog low-pass filter magnitude response is shown in Figure 5.2. It is a 7th order of butterworth filter with parameters, W_p, W_s, R_p and R_s, where, W_p is the passband edge angular frequency in rad/sec, W_s is the stopband edge angular frequency in rad/sec, R_p is the maximum passband attenuation in dB and R_s is the maximum stopband attenuation in dB. The figure is plotted assuming W_p equal to 0.06, W_s equal to 0.25, R_p equal to 1 and R_s equal to 83.

As seen in chapter 4, figures 4.3.7-4.3.11 show the spectra of subband signals obtained by passing a single pulse through filter bands. In the following figures, the pulse train in binary PAM modulation replaces the signal UWB pulse. As expected, both of them have a quite similar shape of spectrum.

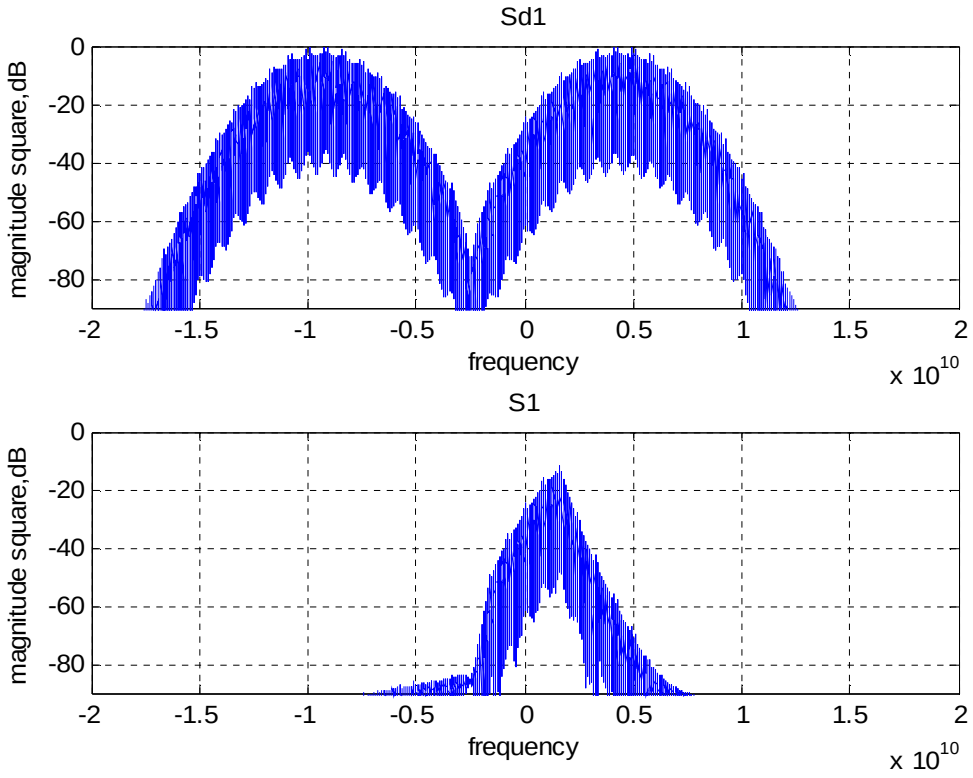

Figure 5.3 Spectra of S1 and S_{d1}

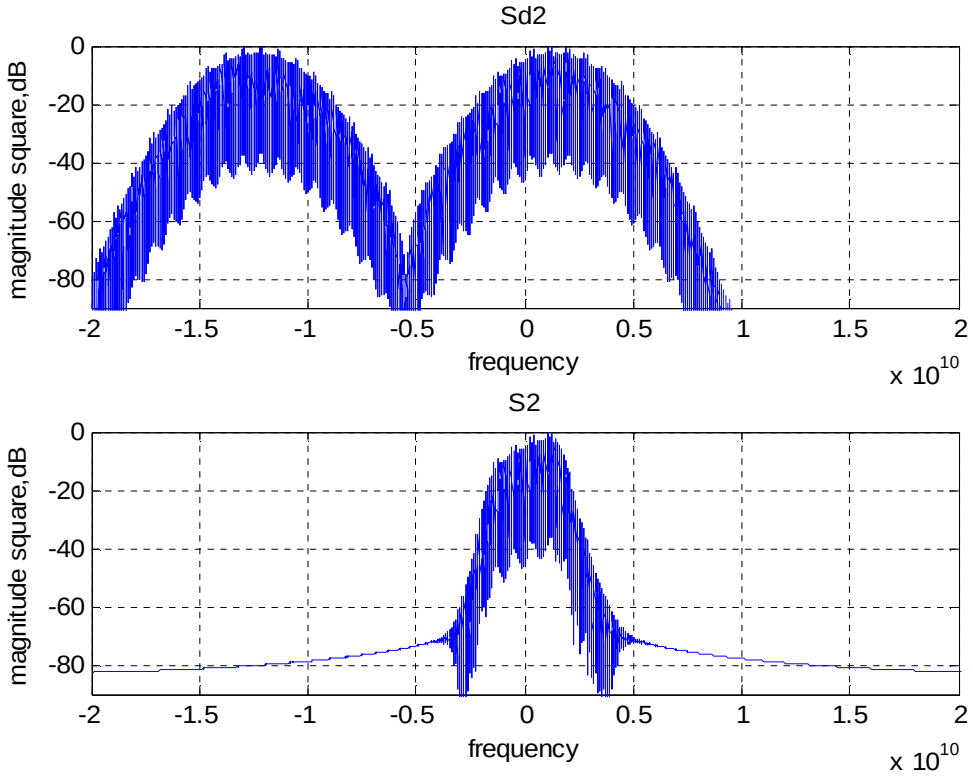

Figure 5.4 Spectra of S1 and S_{d1}

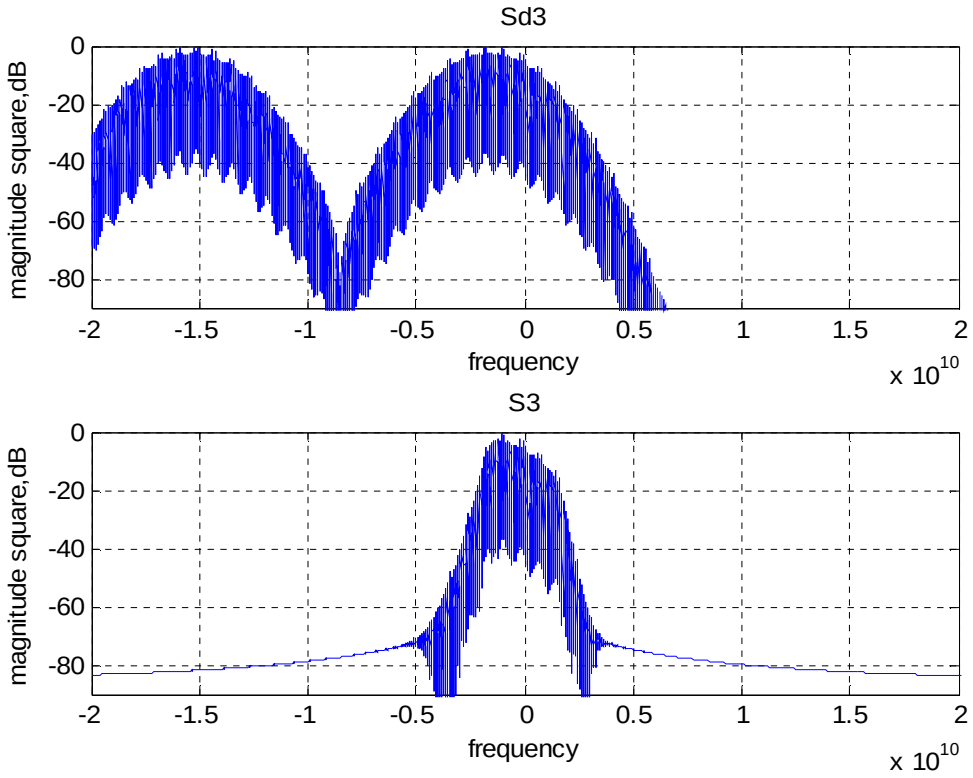

Figure 5.5 Spectra of S1 and S_{d1}

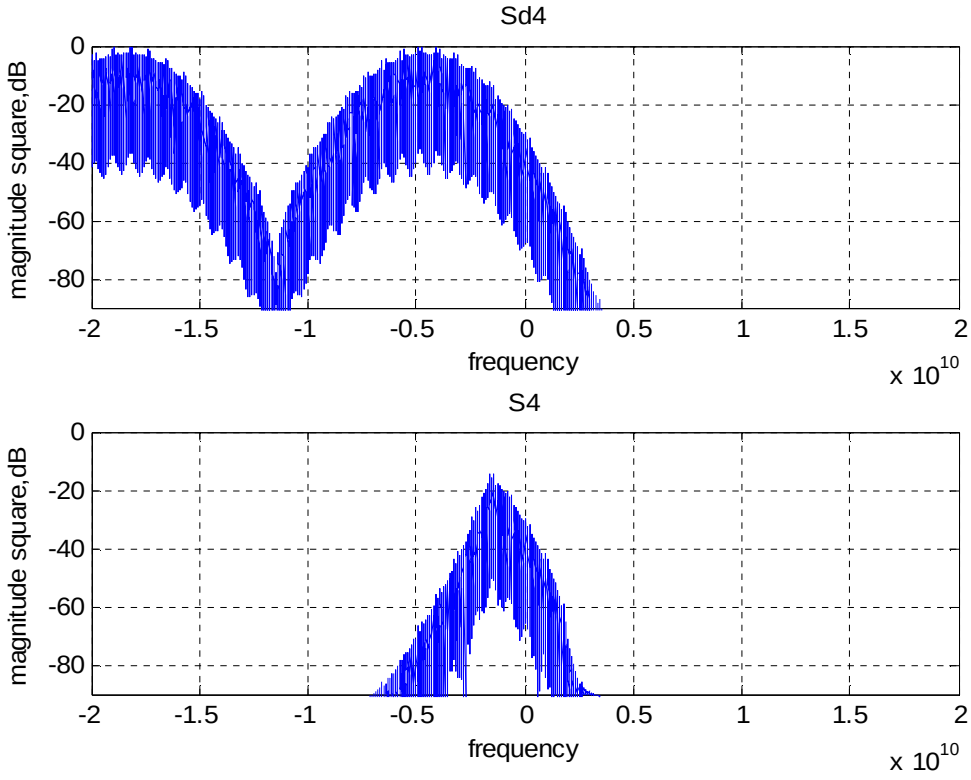

Figure 5.6 Spectra of S1 and S_{d1}

Let us take a look at figures 5.7-5.9. Figure 5.7 shows the subband signals which are down-sampled at the $1/4^{th}$ of sampling frequency f_s. The resulting subband signals are multiplied by exponential functions such that we obtain the outputs of analysis filter bank, y1, y2, y3, y4, shown in the figure 5.8. At synthesis filter banks, the up-sampling operation is applied to the received subband signals for a signal recovery before adaptive filter. Due to the effect of up-sampling, the spectrum is compressed and followed by images.

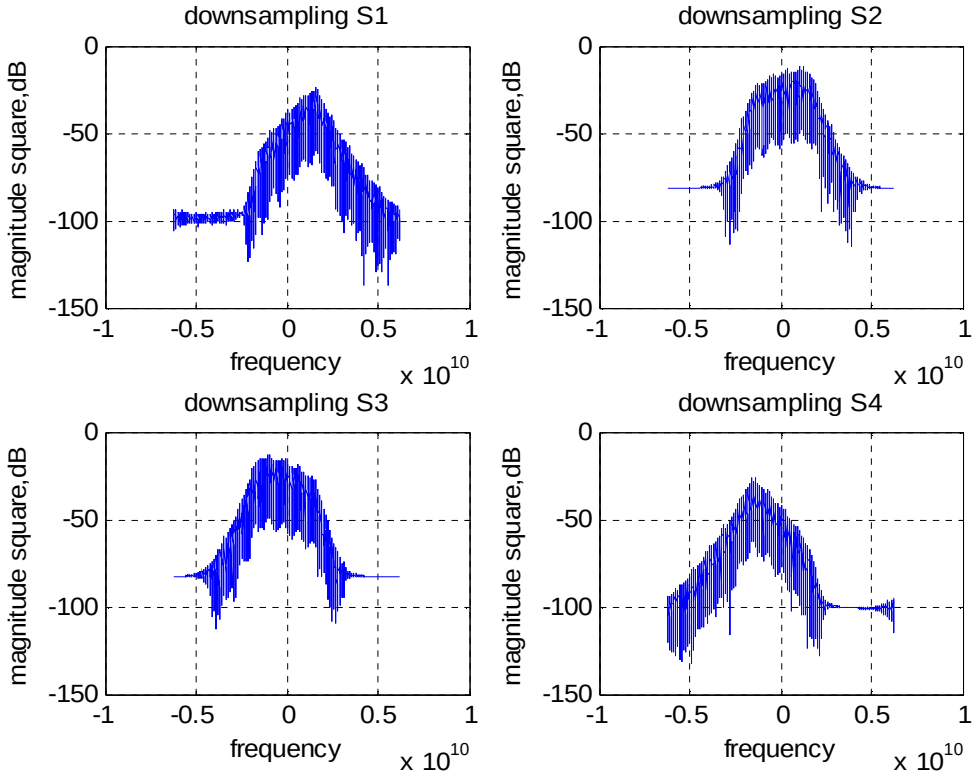

Figure 5.7 Spectra of down-sampling outputs

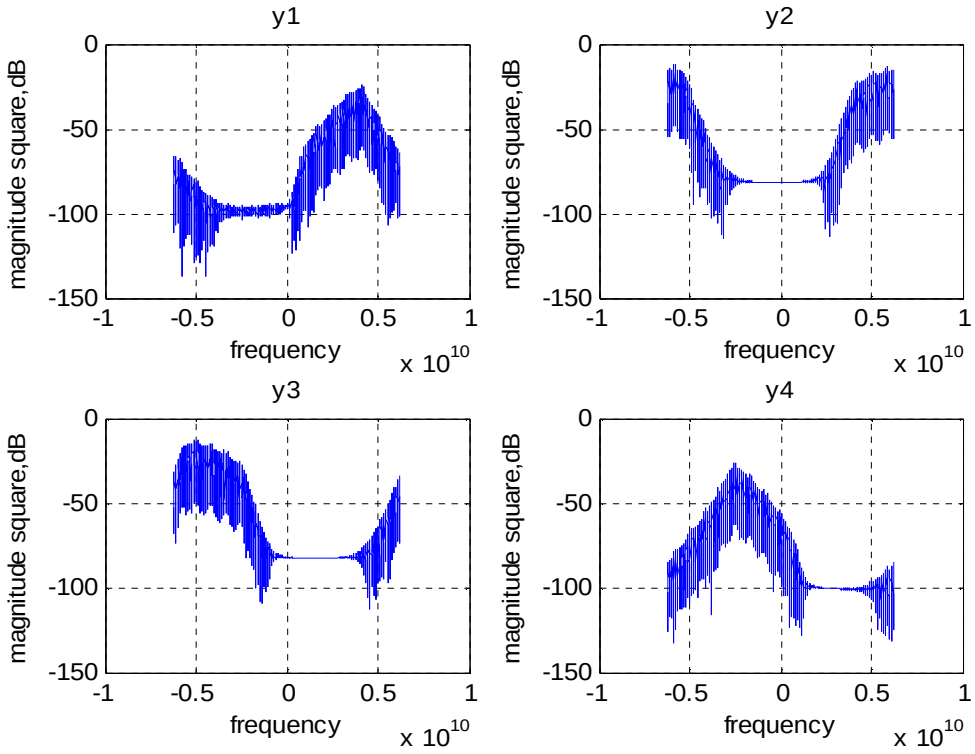

Figure 5.8 Spectra of up-converted outputs

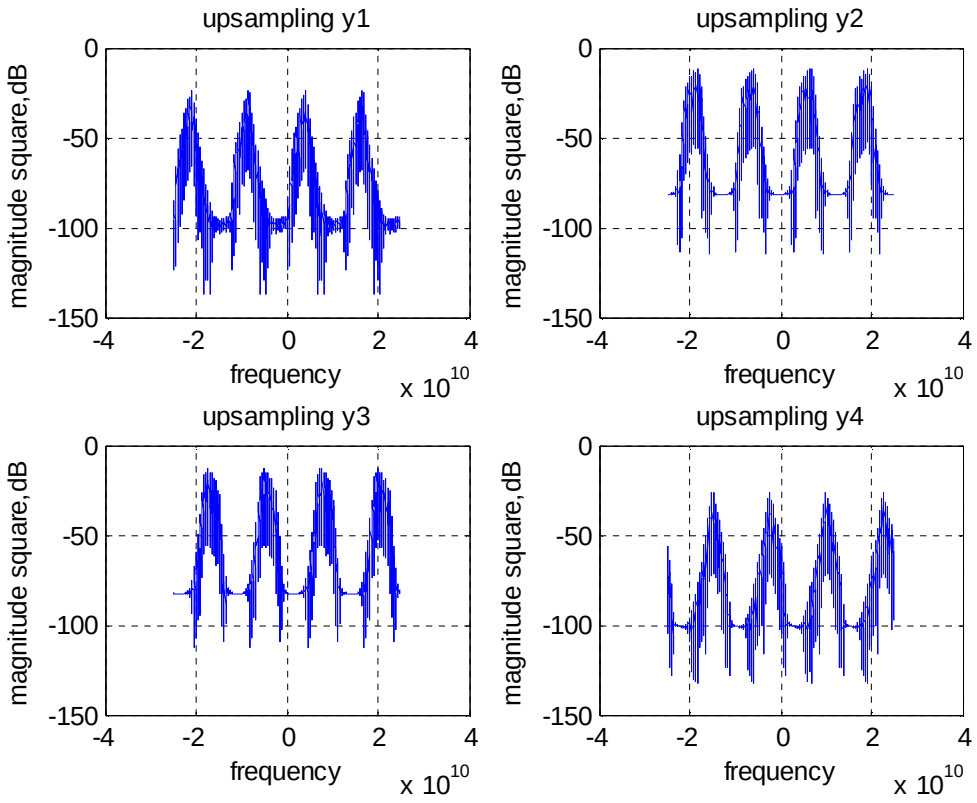

Figure 5.9 Spectra of up-sampling outputs

Figure 5.10 shows system performance with and without channel coding. The dashed line in figure 5.10 shows the performance when convolutional coding with constraint length five and rate ½. Under this condition, each input bit is coded into two output bits for transmission. The simulation is programmed in matlab and uses hard-decision decoding.

Clearly, the convolutionally coded system yields better BER performance, as expected.

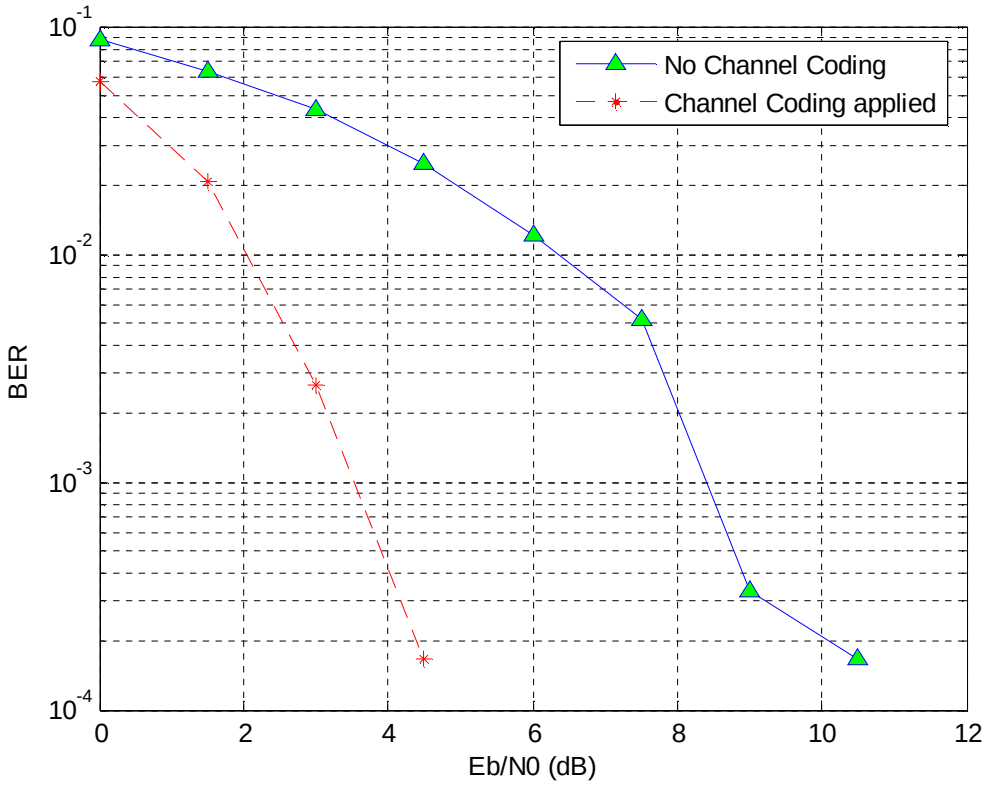

Figure 5.10

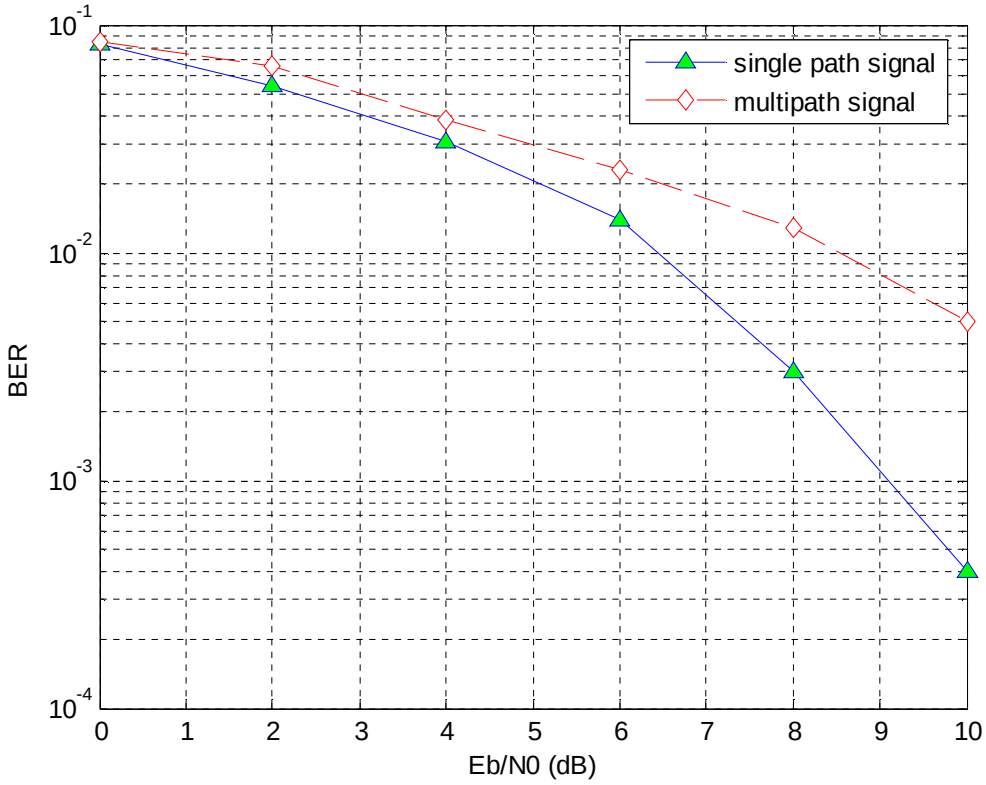

Figure 5.11

Figure 5.11 illustrates the BER performance without channel encoding in single and multipath environments. Because the transmitted signal arrives at the receiver via different propagation paths with different delays, the distortion is caused by a combination of scaled and delayed reflection of the original transmitted signal. As seen in the figure, the BER performance in multipath environment is worse than in single path environment.

The simulation is tested using 3 paths, including the main path and two secondary paths. The main path is the strongest and magnified by gain component. The second and third path is delayed for one and two pulse duration, respectively.

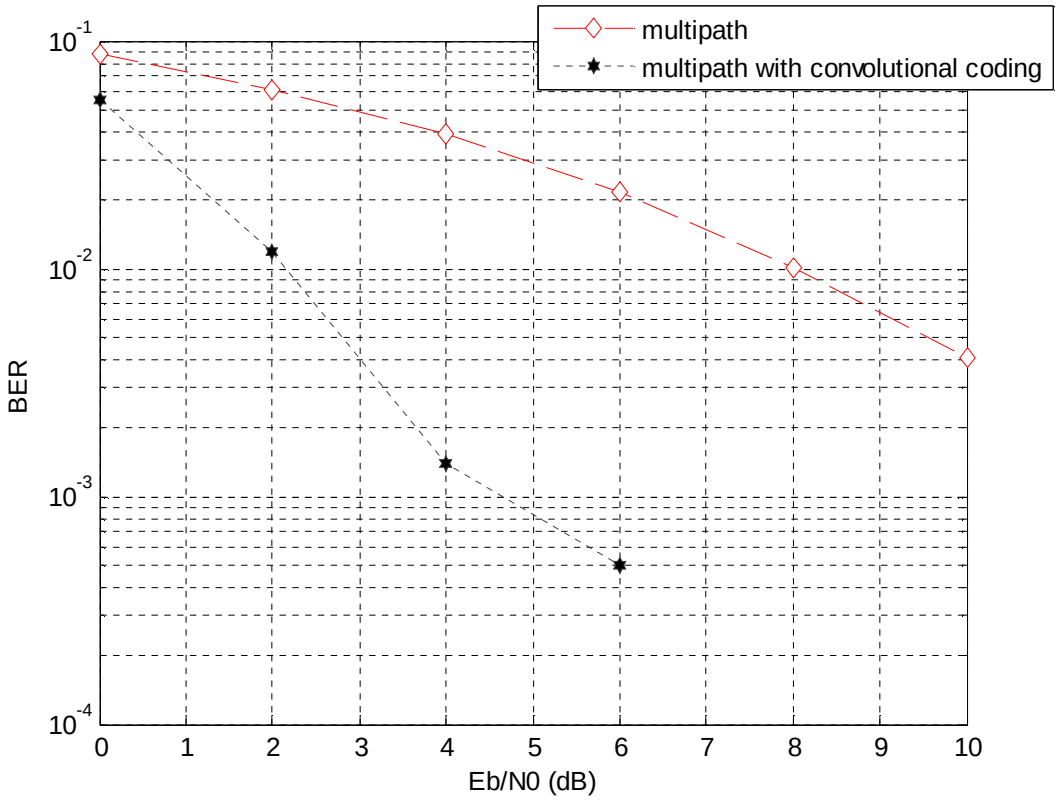

Figure 5.12

Figure 5.12 shows the simulation result in a multipath propagation environment with and without coding. The convolutional encoder has constraint length 5 and rate ½. Again, BER performance in multipath environment is improved by the channel coding technique.

Consider now a new proposed receiver architecture for a multipath propagation environment. Figure 5.13 shows a block diagram shows an implementation of the receiver design. Corresponding to each multipath component, there is a collection of receivers. The information is gathered from different branches and combined together before passing through decision device. The transmitted signal arrives at the receiver with different delays and different attenuations. The coefficients $c0, c1, c2, c3$ in the figure 5.13 are random complex attenuation factors associated with each path.

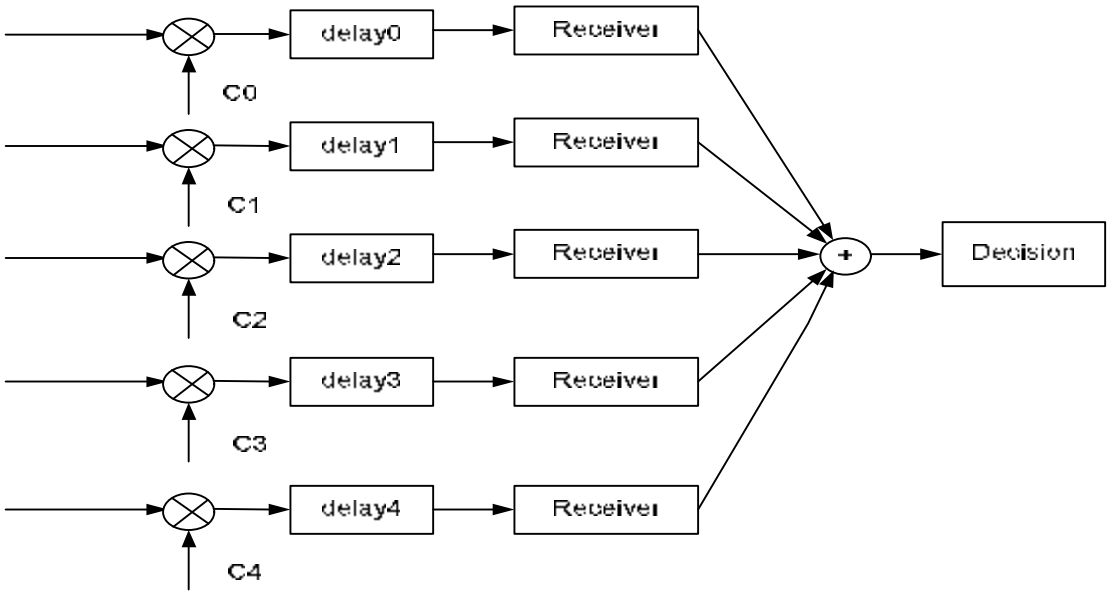

Figure 5.13

For Raleigh fading, the complex multipath coefficient is described by: $c = c_r + j * c_i$, where, c_r and c_i are real-valued Gaussian random variables, with zero mean and 0.5 variance. Figure 5.14 illustrates the variance/power against time delay. As seen, the power relative to each multipath component shows the exponential decay and the fist path has the strongest power.

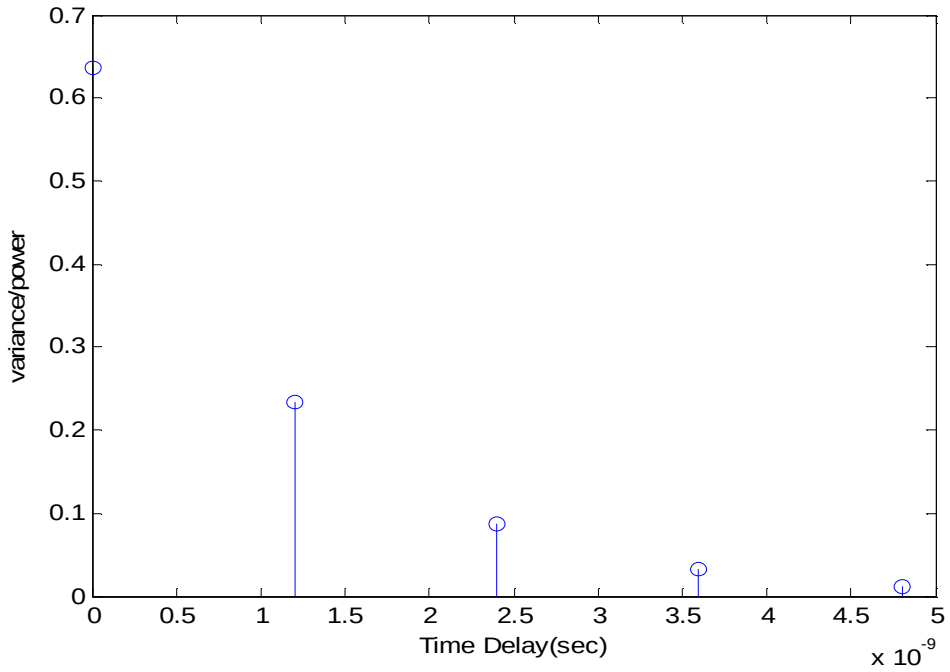

Figure 5.14. power vs. time delay.

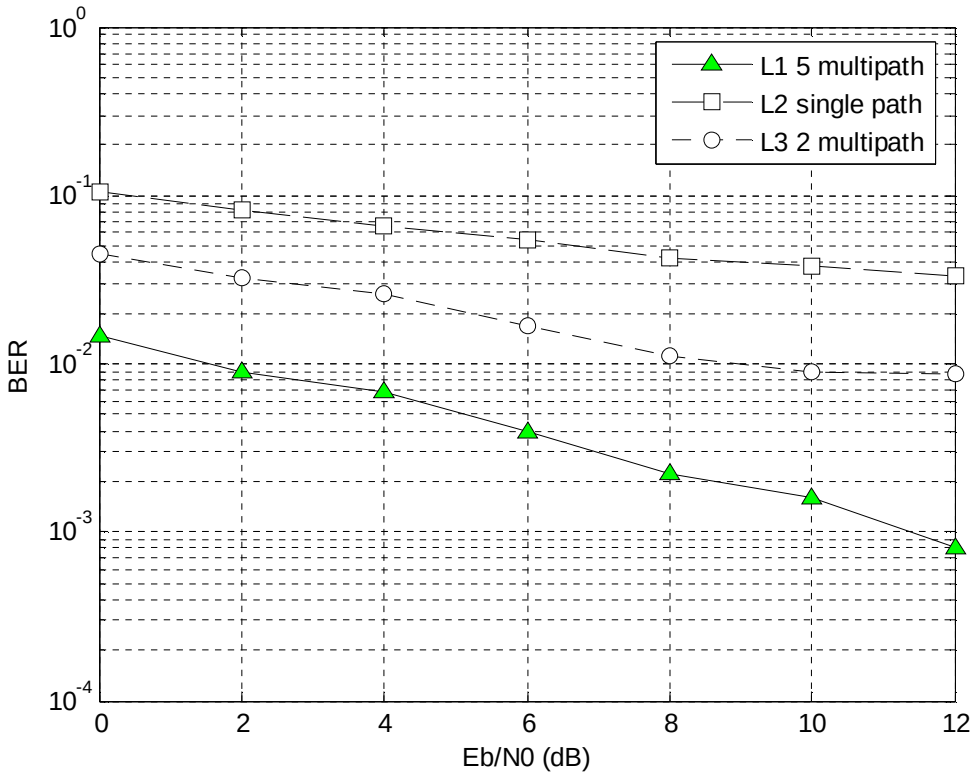

Figure 5.14

The BER performance in multipath with proposed receiver is shown in Figure 5.14. The figure shows system performance for one, two and five paths. As can be seen in figure 5.14, performance improves when the number of paths increases. This is due to the fact that more energy is collected before a decision is made. The following table shows the value of SNR corresponding to BER.

SNR	0	2.0	4.0	6.0	8.0	10.0	12.0
BER of L1	0.0148	0.0089	0.0068	0.0039	0.0022	0.0016	0.0008
BER of L2	0.1063	0.0811	0.0662	0.0549	0.0430	0.0386	0.0335
BER of L3	0.0449	0.0323	0.0259	0.0166	0.0111	0.0090	0.0088

Table 5.1

6. Conclusion

A new frequency channelized receiver architecture for ultra wide band communication systems has been presented. The design herein presented is based on an idea previously conceived by [2]. The contribution of this thesis is the augmentation of the original design, in order to improve performance in a multipath environment.

By using a bank of downconverters and analog low-pass filters, the received UWB signal is channelized into several subbands. Each subband is sampled at the fraction of sampling frequency such that the resolution of ADCs could be considerably relaxed. Moreover, since sharp band-pass filters with high center frequencies are difficult to be implemented in practice, using of low-pass filter simplifies the complexity of receiver design.

Instead of perfectly reconstructing the transmitted signals, the synthesis filters of the channelized receiver perform an MMSE estimate of the transmitted signal optimally. Such synthesis filter can be implemented by using the linear adaptive filter. The existing algorithms are used to adjust the synthesis filter taps to variation in the additive noise and propagation channel. However, the primary disadvantage of adaptive filter is the slow convergence speed.

In a multipath environment, the transmitted signal arrives at the receiver via different propagation paths associated with different time delays. In the proposed multipath receiver structure, each of receivers corresponds to different multipath components with different time delays. The energy is collected before a decision is made. As the number of multipath components increases, the decision device combines more information gathered from each path and makes decisions accurately. Consequently, we can obtain better BER performance.

Finally, a certain amount of future work left. For example, the multi-user case has not yet been addressed.

BIBLIOGRAPHY

[1] National Semiconductor, Analog-data converter, Available: *http://www.national.com/pf/AD/ADC081000.html*

[2] Won Namgoong, *A channelized Digital Ultrawideband Receiver,* IEEE Transactions on wireless communication, vol.2, No3, May 2003

[3] O.Oliaei, *Asymptotically perfect reconstruction in hybrid filter banks,* in Proc. IEEE Int. Conf. Acoustics, Speech, Signal Processing, vol. 3, 1998, pp. 1829-1832

[4] S.Haykin, *Adaptive Filter theory, 3rd ed*. Englewood Clifffs, NJ: Prentice-Hall, 1996.

[5] P.P Vadynathan, *Multirate Systems and Filter Banks,* Englewood Cliffs, NJ: Prentice-Hall ,1993

[6] Scott R Velazquez, Truong Q. Nguyen, *Design of Hybrid filter banks for Analog/Digital Conversion*, IEEE Transaction on signal processing, vol. 46, No.4, April 1998

[7] M. Vetterli, *A theory of multirate filter banks*, IEEE Trans. Acoust., Speech, Signal Processing, vol. ASSP-35, pp. 356–372, Mar. 1987.

[8] M. J. Smith and T. P. Barnwell, III, *Exact reconstruction techniques for tree-structured subband coders*, IEEE Trans. Acoust., Speech, Signal Processing, vol. ASSP-34, pp. 434–441, June 1986.

[9] Richard B. Wells, *Applied coding and Information Theory for Engineers*, NJ: Prentice-Hall 1999

[10] J.Han and C. Nguyen, *A new ultra-wideband, ultra-short monocycle pulse generator with reduced ringing*, IEEE Microwave and Wireless Components Letters, vol.12 No. 6, pp.206-208, June 2002

[11] John G. Proakis, Masoud Salehi, Gerhard Bauch, *Contemporary Communication systems 2nd Edition*, Brooks/Cole 2004

[12] Aaron Michael Orndorff, *Transceiver Design for ultra-wideband Communications*, Blacksburg, VA : Virginia Polytechnic Institute and State University, May 2004

[13] Sanjit K. Mitra, *Digital Signal Processing 2nd Edition*, McGraw-Hill Companies, Inc. 2001

[14] John G. Proakis, *Digital Communications 4th Edition*, McGraw-Hill Companies, Inc. 2001

[15] Authorization of Ultrawideband Technology, First Report and Order, Federal Communication Commission, February 14, 2002

[16] Douglas Jones, *Discrete-Time, Causal Wiener Filter*, Connexions 2003

[17] Robert Morelos-Zaragoza, *Ultra-wideband: A new paradigm in wireless communicaiotns*, San Jose state University, March 11, 2004

[18] Lei Feng, Won Namgoong, *An Oversampled Channelized UWB Receiver with Transmitted Reference Modulation*, Transcations on wireless communications, vol.x, No. x, 2005.

[19] John G. Proakis, Masoud Salehi, *Communication Systems Engineering 2nd Edition*, Prentice-Hall, Inc.2002

[20] A. Montijo and K. Rush, Accuracy in interleaved ADC systems, Hewlett-Packard J., Oct 1993, pp. 36-42.

[21] Mohammad Azizur RAHMAN, Shigenobu SASAKI, Jie ZHOU and Hisakazu KIKUCHI, *On Rake Reception of Ultra Wideband Signal over Multipath Channels from Energy Capture Perspective*, IEICE TRANS. FUNDAMENTALS, vol.E88-A, NO.9, Sep 2005